

## Structural Restorations of the Complete Conjugate US-Mexico Eastern Gulf of Mexico Margin



### Key Points:

- We present sequential structural restorations with flexural backstripping of the post-rift eastern GoM conjugate US-MX margin from Mesozoic to present
- We interpret the geometry and bathymetry of the restored Mesozoic salt basin
- Our analysis indicates significant and widespread Mesozoic anomalous subsidence

### Supporting Information:

Supporting Information may be found in the online version of this article.

### Correspondence to:


M. E. Curry,  
[mcurry2@ncsu.edu](mailto:mcurry2@ncsu.edu)

### Citation:

Curry, M. E., Hudec, M. R., Peel, F. J., Fernandez, N., Apps, G., & Snedden, J. W. (2024). Structural restorations of the complete conjugate US-Mexico eastern Gulf of Mexico margin. *Tectonics*, 43, e2023TC007897. <https://doi.org/10.1029/2023TC007897>

Received 19 APR 2023

Accepted 9 DEC 2023

Magdalena Ellis Curry<sup>1</sup> , Michael R. Hudec<sup>2</sup>, Frank J. Peel<sup>2</sup>, Naiara Fernandez<sup>3</sup>, Gillian Apps<sup>2</sup>, and John W. Snedden<sup>4</sup>

<sup>1</sup>Department of Marine, Earth, and Atmospheric Sciences, North Carolina State University, Raleigh, NC, USA, <sup>2</sup>Jackson School of Geosciences, Bureau of Economic Geology, The University of Texas at Austin, Austin, TX, USA, <sup>3</sup>Hemholtz Centre Potsdam, GFZ German Research Centre for Geosciences, Potsdam, Germany, <sup>4</sup>Jackson School of Geosciences, Institute for Geophysics, The University of Texas at Austin, Austin, TX, USA

**Abstract** We present the first sequential structural restoration with flexural backstripping of the Gulf of Mexico US-Mexico conjugate margin salt basin. We construct four large-scale (100s of km) balanced, sequential structural restorations to investigate spatio-temporal patterns of subsidence, geometry of the original salt basin, feedbacks between post-salt structural and stratigraphic evolution, paleo-bathymetry, and crustal configurations. The restorations are based on interpretations of 2D and 3D seismic data, and include sequential sedimentary decompaction, flexural isostatic backstripping, and thermal isostatic corrections. The spatially variable crustal thinning factor is directly measured from seismic data, and lithologic parameters are determined by well penetrations. We present a model for the original salt basin and discuss evidence for and implications of a deep water salt basin setting for the GoM. Our analysis suggests a salt basin that contained ~1–2 km thick salt in a basin 175–390 km across with ~1 km of bathymetry after salt deposition. The base of salt is mostly smooth with <1 km of local relief in the form of normal faults that disrupt a pre-salt sedimentary section. We find that supra-salt extension and shortening are not balanced, with measurable extension exceeding shortening by 18–30 km on each cross-section. Our subsidence analysis reveals anomalous subsidence totaling 1–2 km during Late Jurassic and Early Cretaceous times that may reflect dynamic topography or depth-dependent thinning. We offer an interpretation of crustal breakup invoking pre-salt clastic sedimentation, salt deposition in a deep water syn-thinning basin, and post-salt lower-crustal exhumation.

**Plain Language Summary** The Gulf of Mexico is a large basin that formed over 200 million years ago due to tectonically driven extension of a supercontinent. Early in its formation it accumulated thick salt deposits. Due to that salt and the later deposition of several kilometers of sedimentary rock that conceal the deep geology, it is difficult to know exactly how extension started and progressed. This study uses new 2D and 3D seismic data that images the deep geology corresponding to that early extension. We sequentially remove each rock layer to reconstruct what the margin looked like in the Mesozoic. By systematically moving back in time we are able to reconstruct the changing geometry, deformation, and bathymetry of the Gulf of Mexico. Our results reveal periods of time when the bathymetry was influenced by unknown factors, which we posit reflects mantle forces.

## 1. Introduction

The Gulf of Mexico (GoM) began forming during Mesozoic rifting of Pangea (Figure 1). The basin contains up to 15 km of syn- and post-rift sediment, including several kilometers of mobile salt that facilitates gravity-driven salt tectonics and obscures much of the subsalt geology (Galloway, 2008; Hudec, Norton, et al., 2013; Peel et al., 1995; Rowan, 2017). The geology of the U.S. GoM margin has been the focus of detailed study with abundant subsurface data and over a century of hydrocarbon exploration and production (Snedden et al., 2020). Less attention has been paid to the Mexican conjugate margin due to historical scarcity of available data. As a result, the relationships between structures on the U.S. and Mexican margins remain speculative. With recent availability of seismic data in offshore Mexico, we can now investigate the structural coevolution of the two sides of the margin. The GoM has been a continuous sink for sediment shed from the North American continent since Mesozoic rifting, and the sedimentary and structural record within the basin contains a complete record of post-rift subsidence. The large spatial scale and high resolution of subsurface data allow a unique analysis of the

© 2024. The Authors.

This is an open access article under the terms of the [Creative Commons Attribution-NonCommercial-NoDerivs License](https://creativecommons.org/licenses/by-nc-nd/4.0/), which permits use and distribution in any medium, provided the original work is properly cited, the use is non-commercial and no modifications or adaptations are made.

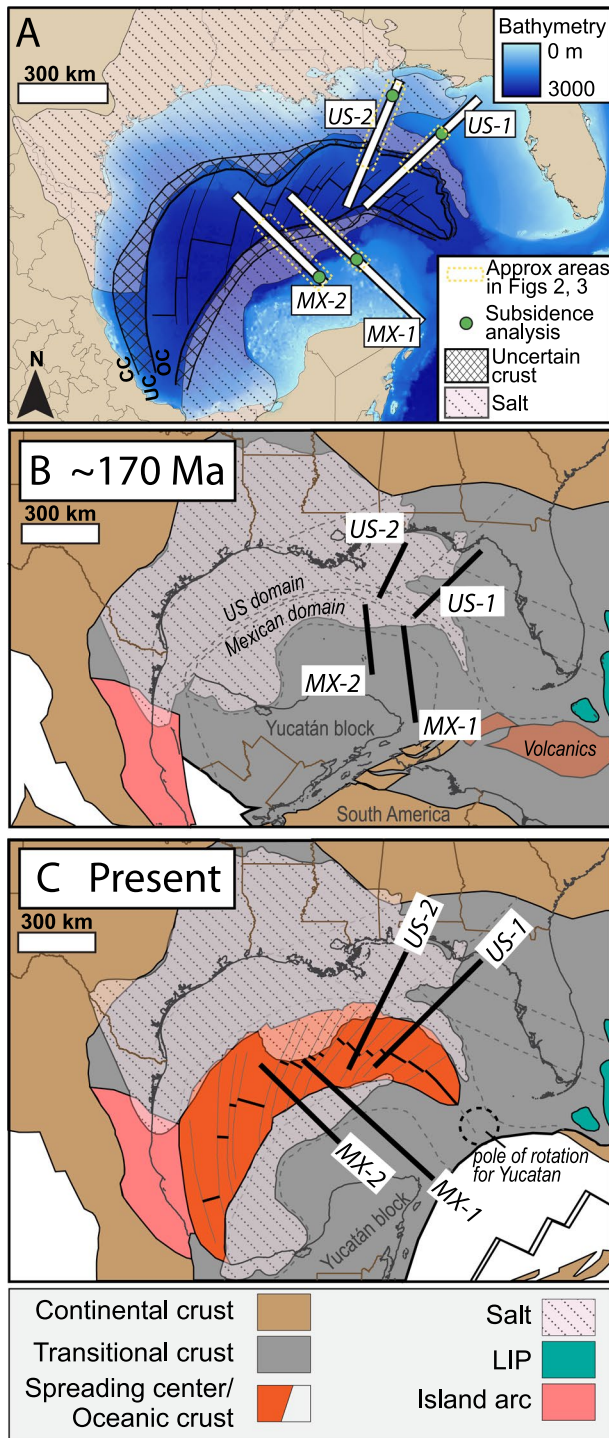


**Figure 1.** Regional details of the GoM. (a) Bathymetry, salt, and crustal limits. White lines show approximate extent of 2D seismic lines that form the basis for the four cross-sections; yellow dashed boxes indicate the approximate extents of the lines shown in Figures 2 and 3. OC = Oceanic crust, CC = Continental crust, UC = Uncertain crust. Tectonic reconstruction at (b) 170 Ma and (c) present from Lawver et al. (2017) showing conjugate sections prior to and after Yucatán rotation.

structural evolution of a conjugate-margin salt basin, and the vertical movements affecting southeast North America since the Mesozoic.

Our understanding of the geologic evolution of the GoM basin advanced significantly over the last several decades thanks to extensive research, exploration, and production efforts, which have produced an unprecedented amount of subsurface data. Several key publications describe the stratigraphy (Galloway, 2008; Snedden & Galloway, 2019), structural styles (Izquierdo-Llavall et al., 2022; Peel et al., 1995; Rowan et al., 2004), role and nature of salt tectonics (Hudec, Jackson, & Peel, 2013; Hudec et al., 2009; Rowan et al., 1999), and large-scale plate tectonics of the basin (Filina et al., 2022; Hudec, Norton, et al., 2013; Imbert, 2005; Pindell & Kennan, 2009; Pindell et al., 2014; Rowan, 2017). Additionally, physical and numerical models shed light on the diverse and often perplexing geology in the GoM (Costa & Vendeville, 2002; Dooley et al., 2013, 2015), while new technologies are enabling improved imaging and interpretation of the subsalt geology (Peel, 2023).

The combination of poor seismic imaging due to complex salt tectonics and a lack of subsalt well penetrations impedes direct observations of deepwater basement structures and complicates interpretations of early evolutionary stages of the GoM, particularly the paleogeography and paleobathymetry associated with salt deposition. Debates continue regarding (a) the mechanisms responsible for salt accommodation and deposition (Peel, 2023; Pindell & Heyn, 2022), (b) the volume and depth of the original salt deposit (Hudec, Norton, et al., 2013; Pindell et al., 2014; Rowan, 2014), (c) the structural mechanisms responsible for crustal breakup and the timing of breakup relative to salt deposition (Imbert, 2005; Norton et al., 2016; Pindell & Kennan, 2009; Rowan, 2018), and (d) the potential roles of dynamic topography and depth-dependent thinning (DDT). Here, we address these debates using new 2D seismic reflection data from offshore Mexico and existing 2D and 3D seismic reflection data from offshore Florida to build the first sequential structural restoration with flexural backstripping of the post-rift GoM conjugate margin from Jurassic salt deposition to present. Our methodology is rooted in the exceptional basin record, taking a reverse-time top-down approach. We present four new 2D structural restorations, two each from the U.S. and Mexican domains of the GoM.

Anomalous vertical movements in sedimentary basins, that is, those that are not modeled by a simple stretching model (e.g., McKenzie, 1978), can be attributed to depth-dependent thinning (DDT) in which different layers of the lithosphere are variably stretched (e.g., Morley & Westaway, 2006) or dynamic topography related to mantle flow (Davies et al., 2023; Gurnis, 1993; Hoggard et al., 2016). For example, ~0.5–2 km of anomalous subsidence is attributed to dynamic topography in the West Siberian Basin (Vibe et al., 2018), and ca. 1 km in the present day GoM (Hoggard et al., 2016). The key to identifying and accurately classifying such vertical movements in the geologic record is to identify subsidence or surface uplift that cannot be explained with obvious mechanisms. Conducting large-scale (100s of km) structural restorations and incorporating thermal, decompaction, and flexural effects facilitates identification of basin-wide trends in vertical movements. Subsidence in the GoM tends to be attributed to thermal relaxation of the lithosphere, outer marginal collapse (Pindell et al., 2014), and/or flexural isostasy (Curry et al., 2018; Galloway, 2008). Dynamic topography and DDT have also been posited in the GoM (Curry et al., 2018; Hoggard et al., 2016; Liu, 2015; Pindell & Heyn, 2022), but without explicitly establishing the thermal and flexural effects we cannot accurately identify and classify excess subsidence.

By constructing sequential, balanced, structural restorations of the conjugate margins and incorporating flexural isostasy, sediment decompaction, and thermal subsidence calculations, we evaluate (a) the initial geometry and early evolution of the salt basin, (b) the feedbacks between salt tectonics and sedimentation, (c) similarities in the timing and nature of structural behavior in the U.S. and Mexican domains, and (d) the impact of crustal geodynamics on basin development. We present a model for the original salt basin and discuss the evidence for and implications of a deep water salt basin setting for the GoM. We estimate the amount of Jurassic deformation on each section and identify a consistent imbalance between observed extension and compression. We identify 100s of meters of subsidence that cannot be attributed to reasonable estimates for thermal subsidence, flexure, or sediment compaction. Finally, we produce a large-scale, evolving geometric framework for the eastern GoM that has implications for the geodynamics of the region and hydrocarbon potential of the basin.

## 2. Geologic History and Current Setting

The GoM basin formed via two phases of extension that began in the Triassic. First, the supercontinent Pangea rifted in a NW-SE direction as South America moved away from North America (Marton & Buffler, 1994; Pindell & Dewey, 1982). This NW-SE directed extension transitioned to counterclockwise rotation of the Yucatán microplate in the Late Jurassic and was primarily accommodated by seafloor spreading, which ceased in the Early Cretaceous (Marton & Buffler, 1994; Pindell & Kennan, 2009). There is general agreement on the overall tectonic history of the GoM passive margin, but there is no consensus on the degree to which the rift-to-drift transition involved syn-rift volcanism, depth-dependent lithospheric stretching, or mantle exhumation (Curry et al., 2018; Filina et al., 2022).

Since the Jurassic, syn- and post-rifting, the GoM basin has been a major sink for sediment derived from the North American continent with variable depocenters and fluvial sources (Peel et al., 1995; Snedden & Galloway, 2019). We adopt the sequence stratigraphic nomenclature when referring to the key stratigraphic packages in the GoM, which divides stratigraphy into low-frequency depositional supersequences separated by regionally significant maximum flooding surfaces (Table 1; Frazier, 1974; Galloway, 2008; Handford & Loucks, 1993; Snedden & Galloway, 2019). The underlying control for these stratal correlations is biostratigraphy. For critical time periods (i.e., during and immediately following salt deposition) and when seismic resolution permits, we use classic lithostratigraphic terminology (e.g., Smackover, Norphlet, Louann) to distinguish stratal sequences.

Mesozoic rifting of Pangea created a large basin that was periodically isolated from the greater ocean circulation, facilitating rapid (<1 m.y.; Peel, 2023), thick salt deposition within the age window 170–165 Ma (Pindell et al., 2021; Pulham et al., 2019). Poor subsalt seismic resolution and a complete lack of subsalt well penetrations leads to uncertainty of the earliest, presalt phase of basin sedimentation (Ewing & Galloway, 2019). Thus we start our Mesozoic description at the base salt unconformity, upon which lies the Louann salt. The Louann salt comprises up to 4 km of nearly pure halite, with anhydrite along the margins. The Louann is overlain by the thin siliciclastic-dominated Norphlet Formation, containing abundant eolian, sabkha, and playa deposits (Ewing & Galloway, 2019). Continued Oxfordian transgression initiated the first marine sequence in the GoM with the carbonate-dominated Smackover Formation, comprised of basin carbonates and marls. Following the Smackover, Haynesville (HVB) carbonate deposition was ultimately superceded by a change to the siliciclastic dominated Cotton Valley episode (CVK), which included large sandy deltaic systems prograding from major fluvial axes (Ewing & Galloway, 2019). As the sediment spread basinward it formed a marine shelf/slope break into deeper water. The Cretaceous sequences (SH, PW, and NT) are dominated by carbonate deposition, with the establishment of a stable shelf-margin reef system dominated by platform carbonates prograding into slope and basin carbonates (Ewing & Galloway, 2019). These widespread carbonates are thoroughly mapped and described (Ewing & Galloway, 2019, and references therein), and provide strong paleo-bathymetric markers within the study area.

Cenozoic deposition in the GoM is described extensively in the literature (Galloway et al., 2000 and references therein). The Paleocene through Oligocene brought surges of siliciclastic sediment to the GoM via the north-western margin, but most of this sediment did not reach the eastern GoM, where the shelf was slowly subsiding with mixed siliciclastic shelf deposits (Ewing & Galloway, 2019). The Miocene through present saw a shift in source, with surges of siliciclastic sediment being fed from the north and east. In the northeast GoM, the platform remained stable and high with only thin mixed shelf deposits, whereas the deep water was dominated by submarine fan systems (Ewing & Galloway, 2019).

At present day, salt in the GoM is divided into two basins, the Louann in the north (mostly US) and the Campeche in the south (mostly Mexico) (Figure 1). It is accepted that these are parts of a single, formerly contiguous salt

**Table 1**  
*Stratigraphy and Rock Properties*

| Unit                           | Supersequence                 | Rock type code <sup>a</sup> | Rock type proportions <sup>b</sup> | Porosity | Depth coefficient (km <sup>-1</sup> ) | Density (kg/m <sup>3</sup> ) | Age (Ma) |
|--------------------------------|-------------------------------|-----------------------------|------------------------------------|----------|---------------------------------------|------------------------------|----------|
| Plio-Pleistocene Basin         | Plio-Pleistocene              | Sand50-Shale50              | S-50, Sh-50                        | 0.56     | 0.395                                 | 2,610                        | 0        |
| Plio-Pleistocene Platform      |                               | Platform                    | Sh-20, C-80                        | 0.454    | 0.424                                 | 2,712                        | 0        |
| Miocene Basin                  | Miocene                       | Sand50-Shale50              | S-50, Sh-50                        | 0.56     | 0.395                                 | 2,610                        | 5.3      |
| Miocene Platform               |                               | Platform                    | Sh-20, C-80                        | 0.454    | 0.424                                 | 2,712                        | 5.3      |
| Oligocene Basin                | Frio-Vicksburg                | Shale85-Sand15              | S-15, Ah-85                        | 0.609    | 0.4825                                | 2,687                        | 23       |
| Oligocene Platform             |                               | Platform                    | Sh-20, C-80                        | 0.454    | 0.424                                 | 2,712                        | 23       |
| Wilcox Basin                   | Wilcox                        | Sand50-Shale50              | S-50, Sh-50                        | 0.56     | 0.395                                 | 2,610                        | 49       |
| Wilcox Platform                |                               | Platform                    | Sh-20, C-80                        | 0.454    | 0.424                                 | 2,712                        | 49       |
| Upper Cretaceous Basin (NT)    | Navarro-Taylor                | Shale50-Carb50              | Sh-50, C-50                        | 0.52     | 0.46                                  | 2,715                        | 65.5     |
| Upper Cretaceous Platform (NT) |                               | Platform_muddy              | Sh-50, C-50                        | 0.52     | 0.46                                  | 2,715                        | 65.5     |
| Mid-Cretaceous Basin (PW)      | Paluxy/Washita/Fredericksburg | Shale50-Carb50              | Sh-50, C-50                        | 0.52     | 0.46                                  | 2,715                        | 99       |
| Mid-Cretaceous Platform (PW)   |                               | Platform_muddy              | Sh-50, C-50                        | 0.52     | 0.46                                  | 2,715                        | 99       |
| Lower Cretaceous Basin (SH)    | Sligo-Hosston                 | Shale50-Carb50              | Sh-50, C-50                        | 0.52     | 0.46                                  | 2,715                        | 119      |
| Lower Cretaceous Platform (SH) |                               | Platform_muddy              | Sh-50, C-50                        | 0.52     | 0.46                                  | 2,715                        | 119      |
| Jurassic 1 Basin (CVK)         | Cotton Valley-Knowles         | Shale50-Carb50              | Sh-50, C-50                        | 0.52     | 0.46                                  | 2,715                        | 140      |
| Jurassic 1 Platform (CVK)      |                               | Platform_muddy              | Sh-50, C-50                        | 0.52     | 0.46                                  | 2,715                        | 140      |
| Jurassic 2 Basin (HVB)         | Haynesville-Buckner           | Shale50-Carb50              | Sh-50, C-50                        | 0.52     | 0.46                                  | 2,715                        | 152      |
| Jurassic 2 Platform (HVB)      |                               | Platform_muddy              | Sh-50, C-50                        | 0.52     | 0.46                                  | 2,715                        | 152      |
| Jurassic 3 Basin (SMK)         | Smackover                     | Shale50-Carb50              | Sh-50, C-50                        | 0.52     | 0.46                                  | 2,715                        | 156      |
| Jurassic 3 Platform (SMK)      |                               | Platform_muddy              | Sh-50, C-50                        | 0.52     | 0.46                                  | 2,715                        | 156      |
| Jurassic 4 Eolian (NOR)        | Norphlet                      | Sandstone                   | S-100                              | 0.49     | 0.27                                  | 2,500                        | 160      |
| Jurassic 4 Marine (SAK)        | Sakarn                        | Sand50-Shale50              | S-50, Sh-50                        | 0.56     | 0.395                                 | 2,610                        | 160      |
| Salt                           | Louann                        | Salt                        | Salt                               | 0        | 0                                     | 2,200                        | 165      |
| Oceanic Crust                  |                               | Basement-basalt             | Basalt                             | 0.03     | 0                                     | 3,000                        | 166      |
| Subsalt rift sequence          |                               | Sand80-Shale20              | S-80, Sh-20                        | 0.518    | 0.32                                  | 2,544                        | 170      |
| Mantle                         |                               | Basement-basalt             | Mantle                             | 0.02     | 0                                     | 3,300                        | 230      |
| Continental Crust              |                               | Basement-continental        | Granite                            | 0.05     | 0                                     | 2,800                        | 300      |

<sup>a</sup>See Table S1 in Supporting Information S1 for rock type details. <sup>b</sup>S: Sand proportion, Sh: Shale proportion, C: Limestone proportion.

basin that subsequently split by oceanic spreading (Buffler, 1980; Humphris, 1978; Salvador, 1987). The updip depositional pinchout of salt is easily identified on seismic data and base of salt or its equivalent weld is a gently dipping surface with only minor relief (<1 km) until the most distal parts of the basin. In offshore Florida and Yucatan, the base of salt drops abruptly ~0.5–1 km and then steps back up ~1–2 km near the seaward limit of the salt basin. This widely recognized structural low is given different names, and different interpretations, in the literature (e.g., Hudec & Norton, 2019; Imbert, 2005; Pindell et al., 2014; Rowan et al., 2000). Here we use the general term “outer trough” to refer to this downdip structural low (Hudec & Norton, 2019) that exhibits more structural relief than updip regions and contains discontinuous, often mobile salt.

### 3. Methods

#### 3.1. Data and Cross-Section Construction

We construct four cross-sections based on 2D seismic lines, supplemented by 3D seismic images where available (Figures 1 and 2; TGS, 2016). The basis for our interpretation is the Gulf of Mexico Basin Depositional Synthesis (GBDS) consortium database, which includes 2,169 wells (764 with Mesozoic tops) and >249,000 km

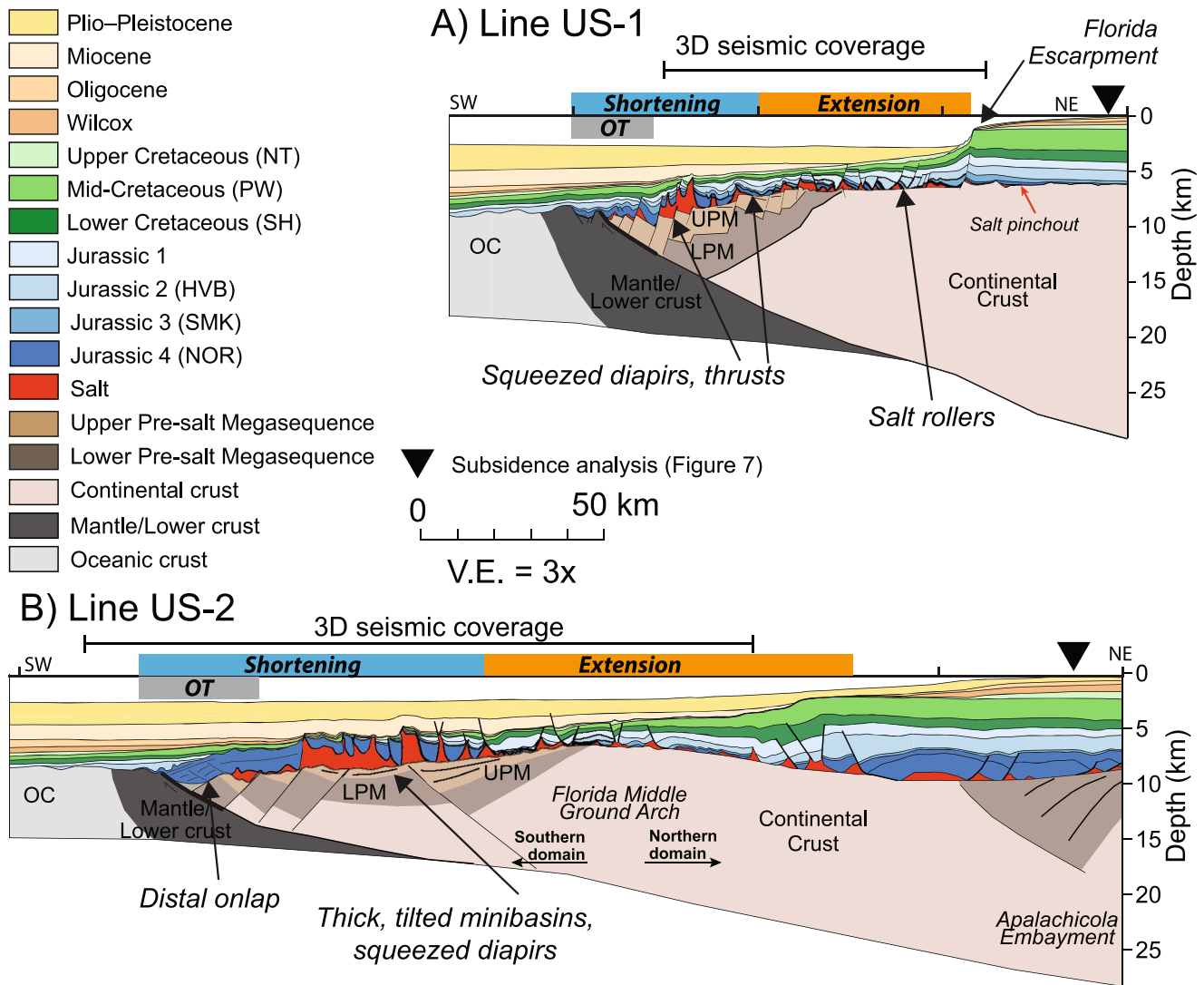


**Figure 2.** Present-day interpretations and key features of lines (a) US-1 and (b) US-2. 3D seismic coverage is indicated. OT = Outer trough, UPM = Upper Presalt Megasequence, LPM = Lower Presalt Megasequence. Blue and orange boxes indicate extensional/shortening domains. Black triangles show location of subsidence analyses (Figure 7).

of depth-migrated (Kirchhoff pre-stack depth migrated [PSDM]) 2D seismic data (Figure S1 in Supporting Information S1). Depth migration brings associated errors that may affect our depth estimates. Well formation tops are correlated to seismic interpretations, and key horizon interpretations are carried across the region by tying crossing seismic lines. All formation tops are rooted in biostratigraphic evidence. The seismic data available to us include the ultra-long-offset, deep penetration 2D PSDM SuperCache data set (Dynamic Data Services, 2012) that facilitates interpretation of the Moho, providing constraints on oceanic and continental crustal thicknesses. We also had access to 3D seismic images from the northeast Gulf of Mexico that enabled detailed interpretation in the salt basin.

### 3.2. Structural Restoration

Interpretations of coevolving structures and depositional sequences may be validated with sequential structural restoration of geologic cross-sections. The presence of salt creates uncertainties in the interpretation because salt violates many classic rules of restoration. Salt flow is three-dimensional and moves in and out of the plane of section, the overall volume of salt decreases with time due to dissolution, and salt diapirs can mask extension and

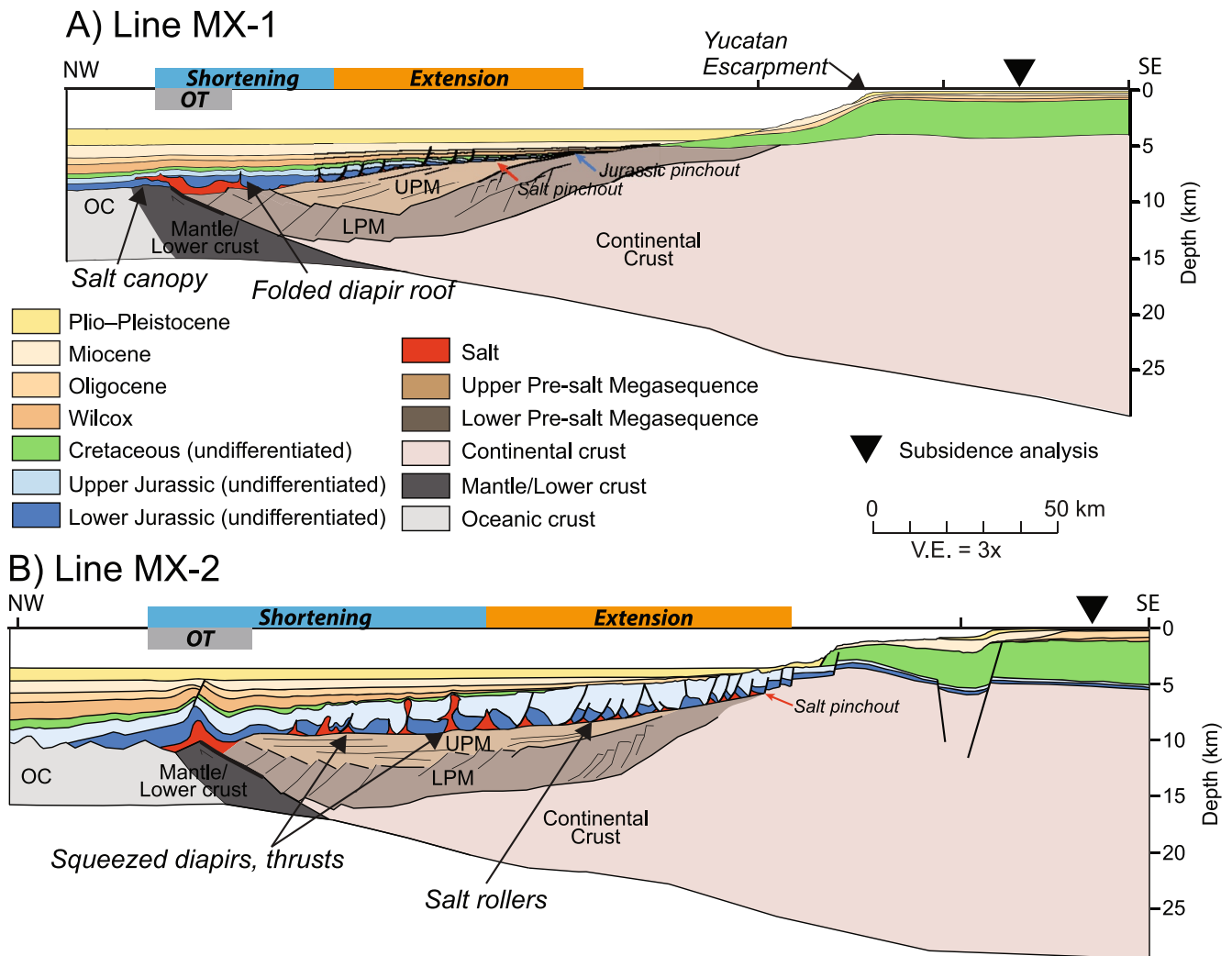


**Figure 3.** Present-day interpretations and key features of lines (a) MX-1 and (b) MX-2. OT = Outer trough, UPM = Upper Presalt Megasequence, LPM = Lower Presalt Megasequence. Blue and orange boxes indicate extensional/shortening domains. Black triangles show location of subsidence analyses (Figure 7).

shortening of adjacent stratigraphy (Rowan & Ratliff, 2012). We refer readers to Rowan and Ratliff (2012) for a thorough discussion of structural restorations in salt basins and challenges and guidelines of the practice. Here, we follow the guidelines laid out by those authors to produce a more robust interpretation, though we acknowledge that conducting 2D restorations in this setting can produce multiple plausible outcomes.

We employ Midland Valley 2D Move™ software to perform our structural restorations (Move Suite, 2016). Following construction of the cross-sections, the sections are sequentially restored at each interpreted depositional sequence (Table 1). At each stratigraphic level, we take the following steps: (a) Backstripping and decompaction, (b) calculate the flexural isostatic effect, (c) calculate the thermal isostatic effect, (d) restore deformation, (e) bathymetric correction. Each step moves the remaining section up vertically. Below we provide details on each step.

### 3.2.1. Backstripping

At each step of the restoration, we utilize backstripping and decompaction algorithms in 2D Move™, which are based on methods of Sclater and Christie (1980). This is a top-down, time-reversed method that involves removing the top-most layer and calculating the decompacted thickness of underlying sediments (Allen & Allen, 2004). For each depositional sequence, we distinguish between the platform and basin lithologies for decompaction (Table 1). The stratigraphy and lithofacies are based on well penetrations from around the basin (Section 3.1 above, Figure S1 in Supporting Information S1).

### 3.2.2. Flexural Isostasy

The lithosphere is strong and able to store elastic stress over geologic timescales (Allen & Allen, 2004; Turcotte & Schubert, 2014), thus it warps in response to applied loads including water, sediment, and volcanism. Our model incorporates a flexural isostatic correction, the wavelength and magnitude of which depends on the load and the effective elastic thickness (Turcotte & Schubert, 2014; parameters in Table S2 of the Supporting Information S1).

### 3.2.3. Thermal Isostasy

Thermal isostatic corrections are controlled by the lithospheric stretching factor ( $\beta$ ; McKenzie, 1978). We assume that crust and mantle stretching factors are equal, and use a crustal thinning factor (original crustal thickness/observed crustal thickness) based on direct measurements from seismic data. In our study area unextended crust is ~35–40 km thick (Huerta & Harry, 2012; Sawyer et al., 1991). Our data quality allow high-density crustal thickness measurements and we use a spatially variable crustal thinning factor to calculate thermal subsidence (McKenzie, 1978; parameters in Table S2 of the Supporting Information S1, additional details in Figure S3 and S4 of the Supporting Information S1).

### 3.2.4. Deformation

We use a combination of simple shear and flexural slip algorithms for move on faults, depending on the interpretation. For example, during the Jurassic, extension was accommodated by rotation of fault blocks over the salt decollement, which demands a flexural slip approach. Linked extensional-shortening domains should contain equivalent updip extension and downdip contraction. In a section with no salt, this equivalence may be easily observed. However, in a salt province, salt diapirs can widen or narrow, salt can flow in a canopy, and/or move out of plane, any of which can result in an imbalance between measurable extension and contraction (Rowan et al., 2004). Here, we refer to this type of deformation as cryptic shortening/extension and identify it on our sections by measuring the imbalance between the visible extension and contraction at each time step.

### 3.2.5. Bathymetric Correction

We utilize paleogeographic maps (Snedden & Galloway, 2019), seismic observations of depositional structures, and sea level curves (Haq et al., 1987) to determine the spatio-temporal variability of water depth throughout the restoration. Mid-to-Late Jurassic sea level can be defined using the earliest Smackover Formation, the first marine interval deposited on top of salt. The Smackover comprises carbonate platform deposits that were drilled closed to its edge and are readily mapped with seismic data. The lowest platform-facies Smackover deposits in the region lie on top of the (sometimes absent) Norphlet Formation, which in turn lies on the depositional top of the Louann Salt. The top of the Louann is, at its edge, within 100 m of the elevation of the lowest identifiable Smackover platform. Paleontological evidence confirms that the Smackover Formation is shallow marine (Heydari et al., 1997) and was connected to the world ocean. The simplest interpretation is that some subsidence occurred during Norphlet deposition, thus the water level of the Louann Salt Sea was close to (<100 m) global sea level.

Up on the platforms, Late Jurassic to Cretaceous deposition was dominated by platform carbonates, providing reliable shallow paleobathymetric constraints. The deep basin Mesozoic paleobathymetry is less certain; after incorporating all the above contributions, we apply the same shift as necessitated in the shallow water. Our paleobathymetric estimate in the distal margin is thus a minimum.

## 3.3. Subsidence Analysis

The workflow outlined above forms the basis for 2D subsidence analyses. For straightforward comparison between lines, we report localized (1D) results on the updip carbonate platform (Figures 2 and 3). We use these updip marginal regions because (a) platform carbonates dominate the Mesozoic, providing strong constraints for paleobathymetry, (b) thermal subsidence is minimal (crustal thinning factors are 1.4–1.9, Figure S4 in Supporting Information S1), and (c) there is no (or minor, in the case of line US-2) supra-salt deformation. We assume negligible erosion because the marginal deposits are submarine and dominantly platform carbonate facies. Additional subsidence mechanisms are necessitated if the top-most unit is not at the appropriate water depth for the lithofacies after going through our flexural backstripping sequence. We refer to this scenario as “anomalous vertical movements.” Because these subsidence analyses are intentionally done outside the salt basin (with the exception of line US-2), positive basement paleo-relief is often observed. Basement relief is interpreted based on seismic data and can be significant. For example, note the relative heights of the basement and the salt pinchout in line MX-1 (Figure 3a).

### 3.4. Salt Basin Reconstruction

The last step of our sequential restoration includes interpreting the original salt basin geometry. Considering the difficulties in conducting restorations in salt provinces and uncertainties regarding salt precipitation in the Mesozoic, we acknowledge that our interpretation is not a unique solution. The following assumptions guide our model: (a) The updip pinchout of salt is pinned at paleo-sea level at the time of salt deposition, (b) we interpret a  $\leq 1^\circ$  slope on the top of salt (a conservative estimate: modern Dead Sea slopes are  $\sim 1\text{--}3^\circ$  (Sirota et al., 2018), Red Sea slopes are  $> 1^\circ$  (Augustin et al., 2014)) consistent with deep-basin halite deposition (e.g., Bqbel & Schreiber, 2014; Hsü, 1972; Peel, 2023; Rowan, 2018) and salt viscosity (Goteti et al., 2013), (c) at the most distal reaches, the depth of top of salt is kept within 200 m for all four section lines based on the presumption that those points were approximate conjugates, and (d) we assume salt dissolution and/or out-of-plane movement reduces the amount of salt through time. The amount of salt dissolution may have been substantial but is impossible to constrain (Kirkham et al., 2020; Sirota et al., 2017). We use the first post-salt deposits as observed in the seismic data to guide the salt level in our model. For example, often the first post-salt deposits are minibasins, thus salt thickness must be sufficient to allow the minibasin to form; ours is thus a minimum estimate (Figure S2 in Supporting Information S1). Adherence to these guidelines involves interpretations regarding salt deposition, details of which are discussed in Section 6.3.

We use the basinward limit of interpreted continental crust as the minimum original salt basin limit; we posit that the continental crust observed sitting below salt must have been in existence at the time of salt deposition because post-salt extension was focused basinward. The modern updip salt pinchout can be confidently assumed to represent the original limit; however, due to gravitational forces, the modern downdip salt limit may not reflect the original limit. We find that after adhering to our guidelines on top salt slope and depth (numbers b and c above), the restored downdip salt limit frequently does not match the modern observation and is farther updip. In these cases, we suggest that the downdip limit of salt migrated basinward through time due to tectonically driven basin widening and/or allochthonous salt flow. Such unconfined seaward flow of salt has been observed in the modern Red Sea (Feldens & Mitchell, 2015; Mitchell et al., 2010; Smith & Santamarina, 2022), and postulated for the GoM (Hudec & Norton, 2019; Rowan, 2018).

## 4. Cross-Section Interpretations and Descriptions

### 4.1. Basement Observations

Historically, the interpretation of presalt and crustal geology has been uncertain due to unclear seismic imaging (e.g., Sawyer et al., 1991), inconclusive potential fields data, and a lack of well penetrations in the deep water. Interpretations have been refined with the availability of improved data (e.g., Eddy et al., 2014; Filina & Beutel, 2021) but significant uncertainties remain (Filina et al., 2022). Here we describe key observations of the subsalt and crustal architecture by broadly characterizing five terrains: (a) oceanic crust, (b) exhumed lower crust/mantle, (c) continental crust, (d) upper presalt megasequence (UPM) and (e) lower presalt megasequence (LPM). The UPM is characterized by semi-transparent, continuous reflectors that are subparallel to the base of salt (Figure 4c), occasionally it is erosionally truncated or deformed by normal faulting (Figures 4a and 4b). The UPM overlies and buries the LPM (Figures 4c and 4d); the boundary between the two is often a bright seismic reflection. The LPM is characterized by higher seismic reflectivity and down-to-the-basin listric normal faults (Figure 4d).

Oceanic crust is identified by a bright, rough reflector at the interface with overlying sediment and a seismic-reflection Moho 6–10 km below the top crustal reflector (Figure 4e). Continental crust is interpreted to be crystalline basement and reaches thicknesses of  $\sim 30\text{--}35$  km in the most proximal imaged stretches. Occasionally, we observe a deep, bright, landward dipping reflector that is interpreted to be the continental Moho. Between oceanic crust and continental crust is a domain characterized by poor seismic imaging and lack of a Moho (Figure 4e). Consistent with other authors (e.g., Filina & Beutel, 2021; Filina & Hartford, 2021; Pindell et al., 2014), we interpret this terrain as either exhumed lower crust or mantle, either of which necessitates crustal-scale exhumation faulting (Figure 4e).

### 4.2. Section US-1

Line US-1 (Figure 2a) is a  $\sim 200$  km long, NE-SW trending section stretching from offshore Florida into the deep water. This line is based on a regional 2D seismic line with supplemental 3D seismic covering the mobile salt



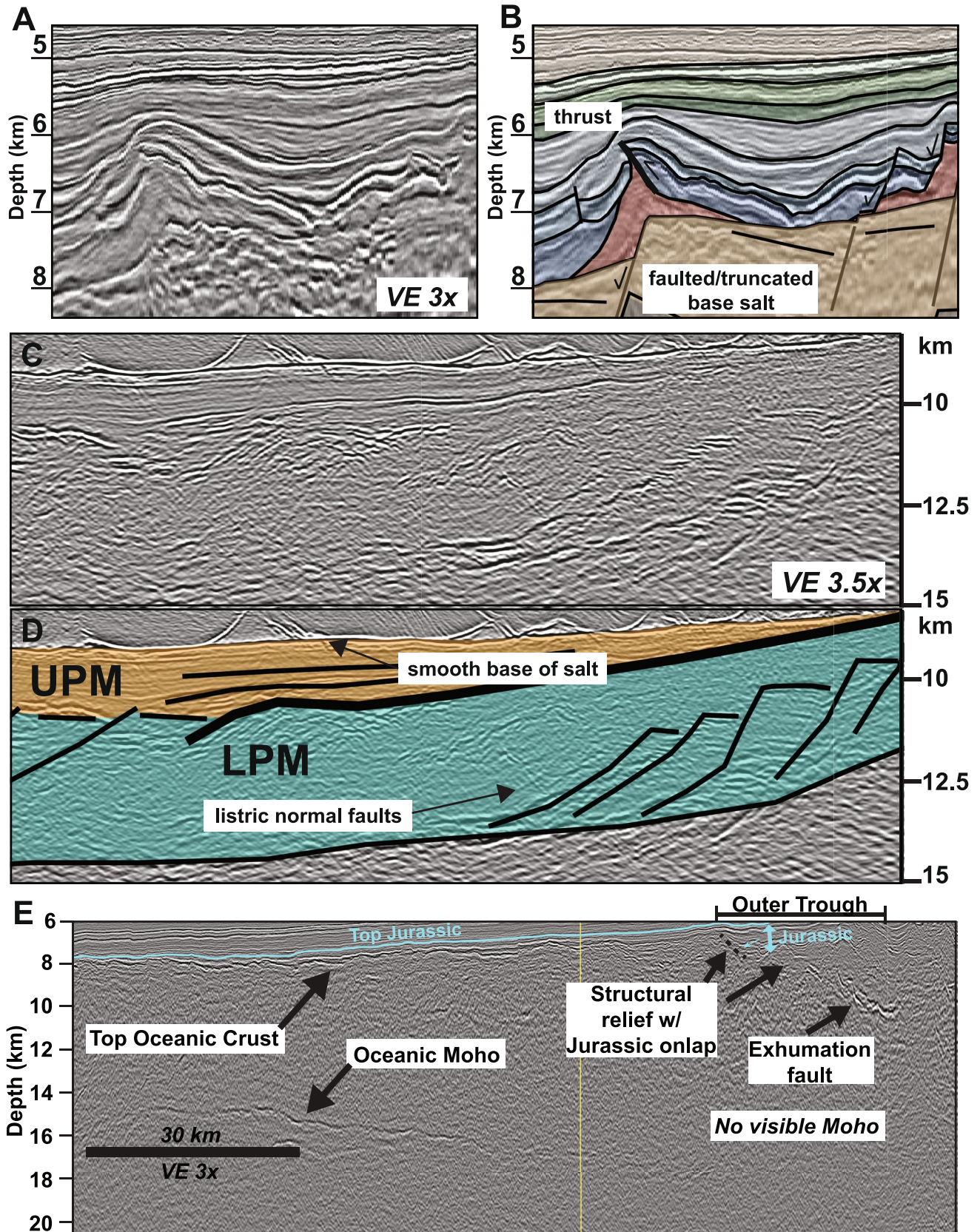


Figure 4.

region. From the updip limit on the Florida platform, the section crosses the Florida Escarpment and ultimately into the oceanic crust domain (Figure 1). From the updip limit on the Florida platform the base of salt dips gently ( $<1^\circ$ ) basinward with no major discontinuities, then dips more steeply ( $3\text{--}4^\circ$ ) and is cut by faulting before crossing into the outer trough (Figure 2a). A distal fault exhumes mantle or lower crust, forming fault-driven relief that influences the distal salt flow. Salt here has a present-day cross-sectional area of  $43\text{ km}^2$ , spanning 130 km along section.

The outer trough is mostly filled with a thick interval of Late Jurassic sediments that subside into and thus postdate the Louann Salt and predate the Smackover Formation. The uppermost part of this section correlates to the continental facies Norphlet Formation, seen in well penetrations further updip (Table 1). The lower part of the section, only observed in the distal downdip regions, has not been drilled. Our interpretation indicates that it consists of clastic sediments that are older than the Norphlet, consistent with the Sakarn Series stratigraphy presented by Rives et al. (2019). This stratigraphic succession displays growth strata onto downdip structural relief (Figure 4).

Moving higher in the stratigraphic section, the units are progressively less affected by salt tectonics. The post-salt Jurassic section has highly variable thickness where it overlies salt, reaching a maximum of 3 km thickness and containing abundant syn-depositional structures. The Cretaceous section is divided into the updip platform carbonates, which reach a thickness of 3.8 km and are undeformed, and downdip units that are much thinner ( $<1\text{ km}$ ) and moderately influenced by salt tectonics.

The Cenozoic units are mostly unaffected by salt tectonics, except for minor deformation adjacent to a salt diapir. On the Florida Platform, the Cenozoic section is  $\leq 1\text{ km}$  thick and discontinuous from basinward counterparts due to the Florida Escarpment. Basinward of the Florida Escarpment, the Cenozoic section reaches a thickness of 6 km in the deepwater and shows progressive onlap onto Cretaceous units.

### 4.3. Section US-2

Line US-2 (Figure 2b) is a  $\sim 300\text{ km}$  long, NNE-SSW striking section stretching from the Alabama-Florida border into deep water (Figure 1). This line is based on a regional 2D seismic line with supplemental 3D seismic covering the mobile salt region. From the updip limit, the section traverses the Apalachicola Embayment then over the nose of the Florida Middle Ground Arch (FMGA) (Figure 2). Due to this basement morphology, it is impossible to situate a cross-section that is a true dip-line throughout the restoration timeframe because the transport direction is nonuniform (Pilcher et al., 2014). It is useful to divide the line into the northern and southern domains, with the crest of the FMGA forming the boundary between the two.

From the northern (i.e., updip) limit on the Florida platform the basement dips  $\sim 3^\circ$  into the Apalachicola Embayment, then rises over the FMGA. From the crest of the FMGA, the basement dips  $\sim 2^\circ$  basinward with minor local relief ( $<1\text{ km}$ ) before crossing into the outer trough. A fault exhumes mantle or lower crust, forming downdip structural relief, eventually transitioning into the oceanic crust domain.

Total section salt has a cross-sectional area of  $140\text{ km}^2$  spanning 260 km along section; in the southern domain the salt cross-section area is  $97\text{ km}^2$  spanning 107 km. The thickness of post-salt Jurassic stratigraphy is influenced by basement relief and salt tectonics. There are abundant syn-depositional structures and minibasins in the down-dip region. The thickness of the first post-salt Jurassic deposits (dark blue, Figure 2) ranges from very thin ( $\sim 100\text{ m}$ ) over the FMGA to  $\sim 2.5\text{ km}$  in the downdip region, where they form thick minibasins. In the northern domain, within the Apalachicola Embayment, Jurassic stratigraphy is up to 5 km thick; in the southern domain the maximum thickness is 2.5 km. The Cretaceous stratigraphy is up to 4 km thick on the platform, decreasing in thickness to  $\sim 100\text{ m}$  in the southern domain where salt tectonics causes faulting and thickness variations (green units, Figure 2).

In the northern domain the Cenozoic section is  $\sim 2\text{ km}$  thick and stable, with no observable deformation. In the southern domain, salt tectonics continues to cause deformation and thinning through the Oligocene, with moderate folding and faulting observable in the Miocene stratigraphy (light beige unit, Figure 2). The Miocene-to-present rocks constitute thick ( $>6.5\text{ km}$ ) stratigraphy in the downdip region.

**Figure 4.** Seismic images of key features. (a) Uninterpreted and (b) interpreted image of 3D seismic data showing contractional structures from the shortening domain of line US1, and faulted and erosionally truncated base of salt. Color bar matches Figure 1. (c) Uninterpreted and (d) interpreted image of 2D seismic data showing seismic character of Upper Presalt Megasequence (UPM, orange) and Lower Presalt Megasequence (LPM, green), as well as a smooth base of salt. (e) Seismic imaging of crustal features from 2D seismic data. Seismic data is depth-migrated and courtesy of TGS (2016).

The basement relief complicates the salt-influenced deformation on this line, and we focus our discussion on the southern domain where salt movement affects stratigraphy as young as the Plio-Pleistocene (Figure 2). There is a region with Jurassic-aged minibasins nearly 5 km thick. The minibasins are younger than the Louann salt and older than the Smackover, equivalent to or immediately predating the Norphlet; later Jurassic stratigraphy is thin to absent over this area. Growth strata in the minibasins are indicative of minor tilting, and the salt diapirs between minibasins contracted and deformed younger stratigraphy. There are both Jurassic and Cretaceous growth-faults, and there is evidence for minor thrust faulting on the downdip boundaries of minibasins (Figure 4).

#### 4.4. Section MX-1

Line MX-1 (Figure 3a) is a ~300 km long, NW-SE striking section stretching from the northeastern-most tip of Yucatán. This interpretation is based on a regional 2D seismic line. From the southern (updip) limit on the Yucatán platform the basement dips basinward 1–2° with no major discontinuities, then dips more steeply (4°) before crossing into the outer trough. A fault exhumes mantle or lower crust creating structural relief, eventually transitioning into the oceanic crust domain.

Basinward of the Yucatán Platform, the Cenozoic section reaches a thickness of ~6 km in the deepwater and shows progressive onlap onto a major unconformity (Figure 3). On the Yucatán Platform the Cenozoic section is ~1 km thick and undeformed. The Yucatán escarpment forms a discontinuity between the basin and platform deposits.

On this line Mesozoic units are affected by salt-detached extensional faulting, which mostly ceased by end Cretaceous. The salt has a cross-sectional area of 17 km<sup>2</sup>, spanning 60 km. The post-salt Jurassic section is thinnest here of all evaluated sections, reaching thicknesses of 1–2 km downdip. Due to poor seismic quality and lack of well control, the Jurassic is not interpreted on the Yucatán Platform. The Cretaceous section is divided into the platform carbonates, which reach a thickness of 3.2 km, and thinner (<1 km) downdip units that are marginally influenced by salt tectonics. At the basinward extent of salt, we interpret a small Mesozoic allochthonous salt canopy (Figure 3).

#### 4.5. Section MX-2

Line MX-2 (Figure 3) is a ~300 km long, NW-SE striking section stretching from offshore Yucatán. Our interpretation is based on a regional 2D seismic line. The deepwater units can be directly correlated across from US seismic interpretations; on the platform interpretations are based on seismic character. Near the southern (i.e., updip) limit on the Yucatán platform there are two basement-involved normal faults (<1 km offset), basinward of which the basement dips ~3° then levels out (<1°) before crossing into the outer trough. A fault exhumes mantle or lower crust, forming fault-driven relief that influences the distal salt flow.

The modern salt here has a cross-sectional area of 45 km<sup>2</sup>, spanning 160 km. The post-salt Jurassic section reaches thicknesses of 3 km in deepwater and contains abundant salt-detached syn-depositional structures (Figure 3). On the Yucatán Platform, the Jurassic is <1 km and not affected by salt tectonics. The Cretaceous section is divided into the platform carbonates, which reach a thickness of 3.8 km, and thin downdip units (<1 km, green units, Figure 3). The downdip Cretaceous section onlaps onto underlying Jurassic and thins over salt diapirs.

Basinward of the Yucatán Platform, the Cenozoic section reaches a thickness of ~6 km in the deepwater and shows progressive onlap onto the Jurassic. The Cenozoic section is mostly undeformed, except for a Miocene-aged, basin-dipping normal fault cutting the crest of a salt-cored fold above the outer trough. On the Yucatán Platform, the Cenozoic section is ~1 km thick and discontinuous from off-platform counterparts.

Basinward of the platform are numerous salt-detached extensional faults, mostly affecting the Mesozoic section. There is evidence of downdip compression in the form of squeezed diapirs and thrust faults (Figures 3 and 4); this linked extension-compression system is mostly confined to the Jurassic, with only minor post-Jurassic deformation observed.

## 5. Results

### 5.1. Restorations

In Figures 5 and 6 we present the Mesozoic stages of our conjugate restorations. We interpret salt deposition occurring synchronous with or immediately following crustal split based on (a) salt thinning toward the distal end of the sections and (b) post-salt sedimentation (Lower Jurassic) onlapping the distal structural relief. Our interpretation shows a period of lower crustal/mantle exhumation between crustal split and emplacement of oceanic

crust, which is based on the seismic character of these crustal domains as discussed above. Below we present details of the original salt basin, key structural elements, and subsidence analyses.

## 5.2. Post-Rift Extension-Shortening

Post-Jurassic extension and shortening are  $<1$  km for all sections, so we focus our investigation on Jurassic deformation. We measure the amount of along-section extension and shortening expressed on each Jurassic horizon and sum them for the total Jurassic deformation. Measured extension is consistently  $\sim 10\times$  higher than shortening, symptomatic of cryptic salt-induced deformation or translation onto newly formed/exhumed crust. Extension ranges from 18.5 to 30 km, whereas observed shortening ranges from 0 to 3 km (Figure 8). On line US-1 (Figure 2), a series of gravity-induced detachment faults accommodate 22 km of extension in the Mesozoic units. There are 3 km of measurable downdip shortening in the form of folded diapir roofs and thrust faults. On line US-2 (Figure 2) we measure 18.5 km of extension in Mesozoic units of the Southern domain; there is evidence of squeezed diapirs but we could not quantify any shortening. On line MX-1 (Figure 3), a series of gravity-induced detachment faults accommodate 21 km of extension in Mesozoic units. There is  $\sim 1$  km of measurable downdip shortening in the form of folded diapir roofs, and a salt canopy that may be driven by contractional and/or gravitational forcing. On line MX-2 (Figure 3), a series of gravity-induced detachment faults accommodate 30 km of extension in Mesozoic units. There are 3 km of downdip shortening in the form of folded diapir roofs and thrust faults.

## 5.3. Salt Basin

The last stage of the restorations shows our model for the salt-basin geometry at the end of salt deposition (Figures 5d and 6d). These interpretations rely on the guidelines and underlying assumptions we describe in Section 3.4. The original autochthonous top of salt has slopes of  $0.3\text{--}1^\circ$ . The maximum original salt thickness on each section is between  $\sim 1$  and 2 km, and the maximum top autochthonous salt depth (equivalent to relief on salt) is  $\sim 1$  km. Salt cross-sectional area decreases from deposition to present; the present salt cross-sectional area as a percent of original salt cross-sectional area ranges from 43% to 80%; the greatest change (43%) is for line MX-2.

The original salt basin was 175 km across in the southeast and 390 km across in the central GoM. From salt deposition to present the along-section length increases (i.e., the salt basin widens) between 4 and 10 km (Figure 8). Lines US-1 and MX-1 have 6 and 8 km of basin widening, respectively (Figures 5 and 8); Lines US-2 and MX-2 have 9 and 10 km, respectively (Figures 6 and 8).

## 5.4. Subsidence Analysis

Subsidence analysis consistently presents a scenario where all considered corrections fail to bring the Mesozoic platform stratigraphy to global sea level, as necessitated by copious stratigraphic evidence (Figures 7 and 8). In each section, after applying thermal and flexural corrections, Mesozoic stratigraphy is situated too deep for deposition of the platform carbonates that make up the stratigraphy. A positive bathymetric correction is thus necessitated. In other words, there is significant subsidence on all the cross-sections with no clear origin. The magnitude of the bathymetric correction varies in space and time, but some general trends are evident (Figure 8). The cumulative amount of anomalous subsidence (i.e., the sum of anomalous subsidence through time) ranges from 1.7 to 2.5 km. Moving backwards in time from present, there are no significant vertical corrections required until Early Cretaceous, ca. 120 Ma (Figure 8). We only have intra-Cretaceous constraints for U.S. lines, and they show  $\sim 600$  m of excess subsidence in the Early Cretaceous. At the Cretaceous-Jurassic boundary, the Mexican lines necessitate 0.6–1 km of bathymetric corrections, though we note that because we do not have intra-Cretaceous constraints the bathymetric correction applied at the end of the Cretaceous is cumulative for the entire Cretaceous. Furthermore, because Jurassic stratigraphy on line MX-1 pinches out in the basin  $\sim 100$  km away from the subsidence analysis location, we assume that the Cretaceous carbonate stratigraphy begins at the onset of the Cretaceous. The U.S. lines necessitate no significant vertical correction at the Cretaceous-Jurassic boundary, but at ca. 156 Ma a 500–800 m positive shift is required. For the oldest timestep, which represents the final salt basin, bathymetric corrections are necessary on the two Mexican lines ( $\sim 500\text{--}600$  m), and line US-2 ( $\sim 1,000$  m). During these time intervals eustatic sea level was 50–150 m greater than today, insufficient to account for the observations (Haq et al., 1987). In summary, there are at least two periods of time—Early Cretaceous and Late Jurassic—where our restorations require 500–1,000 m of bathymetric corrections (Figure 8).

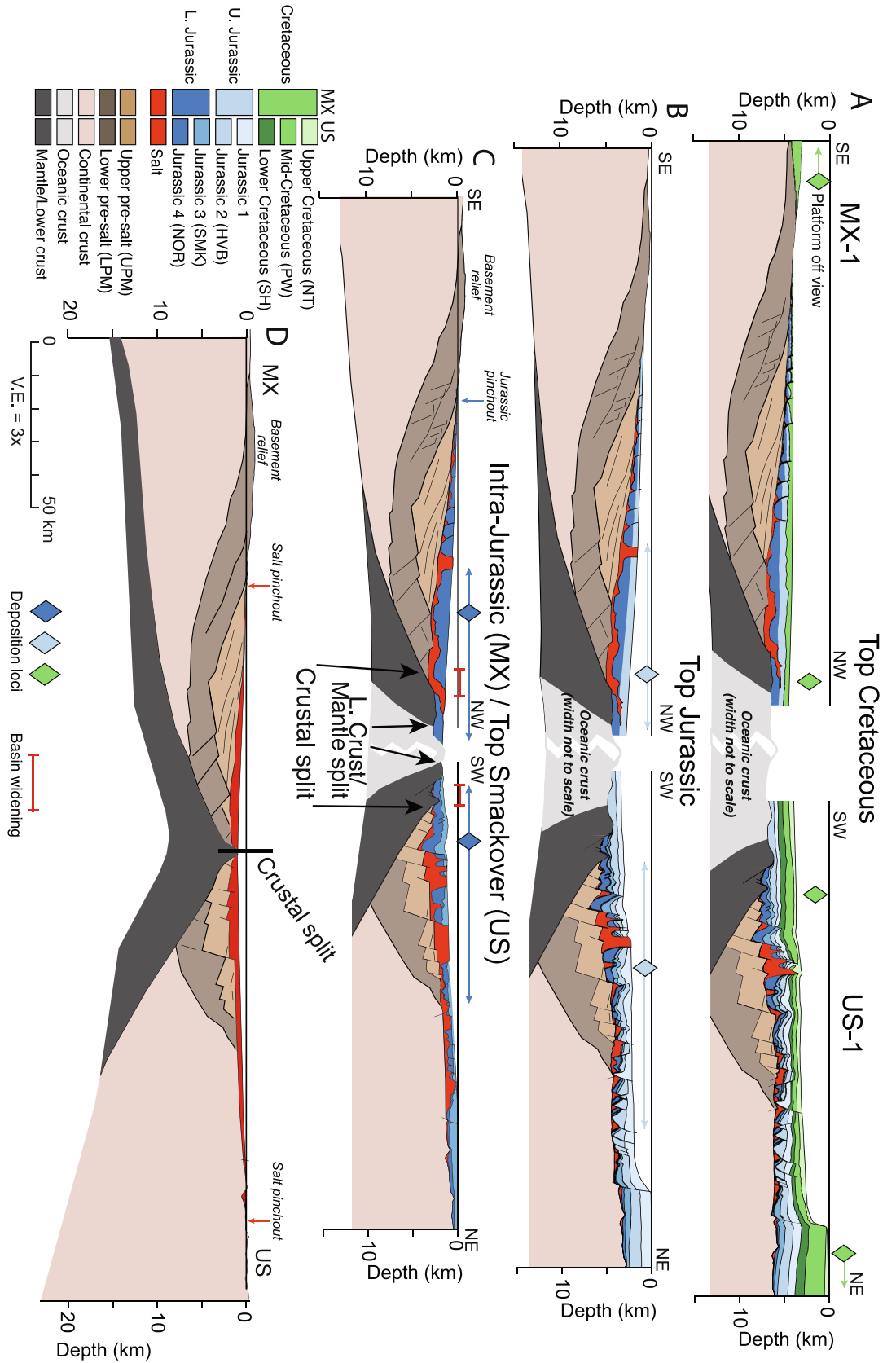


Figure 5. (next page): Mesozoic restoration of conjugate lines US-1 and MX-1.

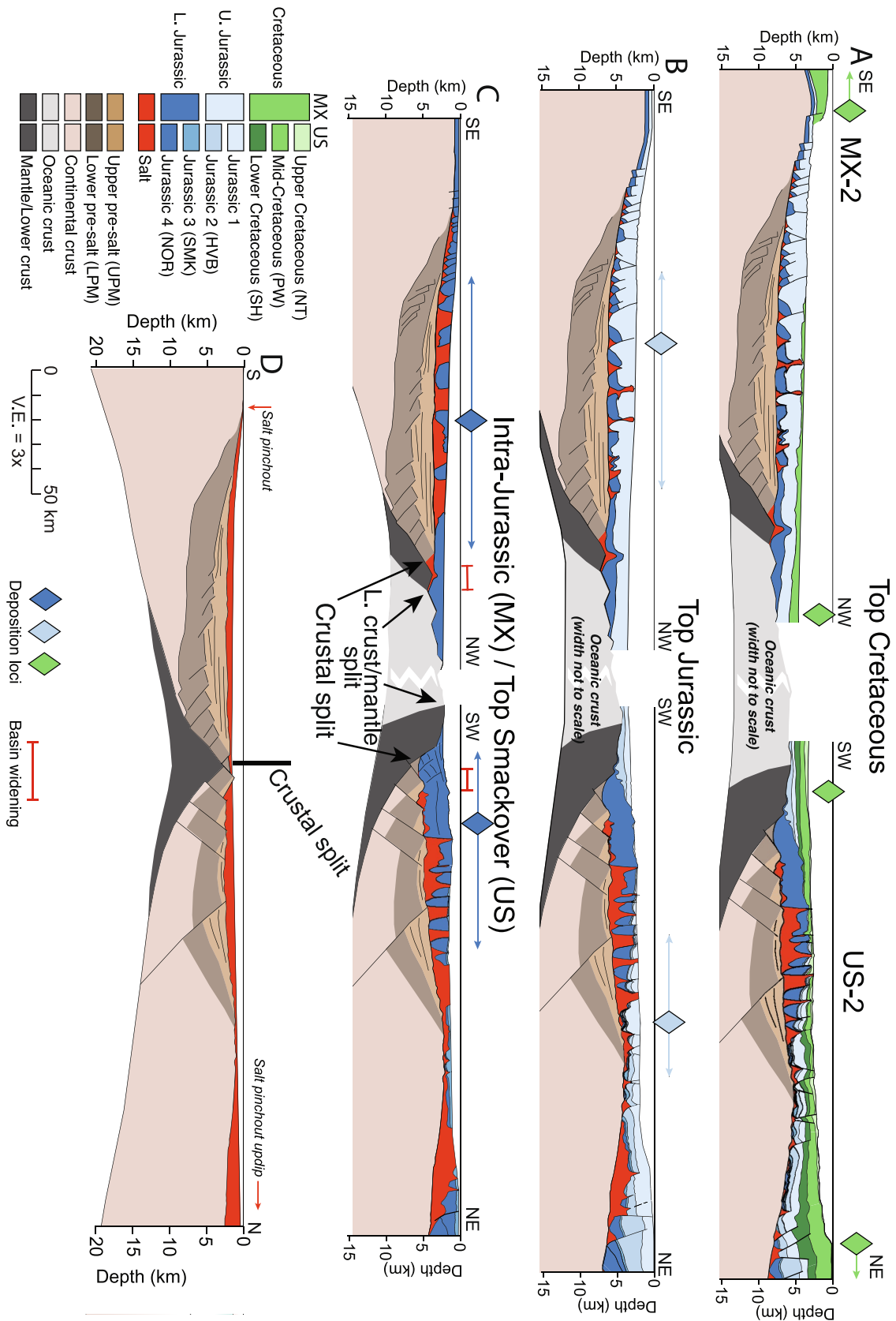
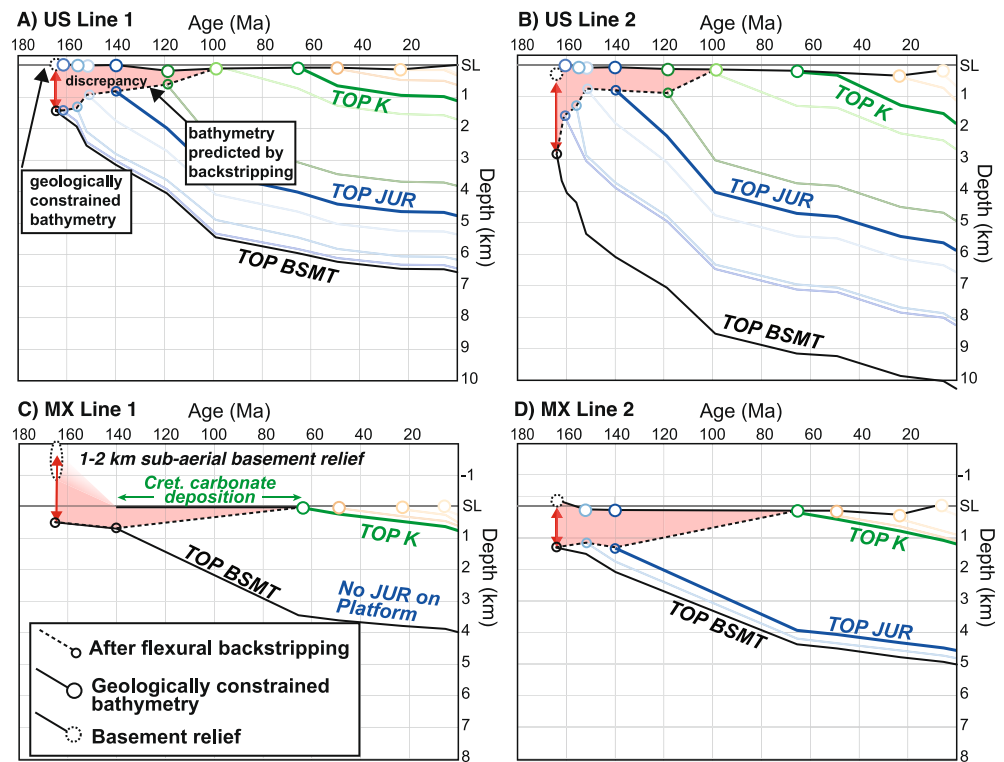


Figure 6. Mesozoic restoration of conjugate lines US-2 and MX-2.



**Figure 7.** Results of subsidence analysis for four points located on the proximal margin within the carbonate platform. Lines show subsidence of formation tops, small circles and dotted lines show predicted bathymetry following flexural backstripping workflow; solid line and large circles represent bathymetry based on environment of deposition; red shading highlights the discrepancy between model and observation. TOP K = Top Cretaceous; TOP JUR = Top Jurassic; TOP BSMT = Base of salt. Additional details in Figure S4 of the Supporting Information S1.

To eliminate the possibility these observations are an artifact of incorrect restoration, we undertook a sensitivity analysis of (a) thermal isostasy, (b) basement lithology, and (c) mud content of post-salt stratigraphy to investigate potential errors in our elevation modeling. To rule out additional thermal isostasy, we evaluate the influence of variable original crustal thicknesses, which effectively increases the crustal thinning factor and thus thermal subsidence (Figure 8c). We consider the subsidence effect of a crystalline versus sedimentary pre-salt section and evaluate the influence of variably mud-rich lithologies in the post-salt section. Increasing the mud component by a factor of 2.5x effectively increases the amount of decompaction (and thus subsidence) by ~100 m. The results, shown in Figure 8c, indicate that none of these potential sources of error are sufficient to bring the basement up to the level indicated by geological evidence, suggesting that the anomaly is a real geodynamic effect.

## 6. Discussion

The four lines presented here are the first to show a full suite of detailed structural restorations with comprehensive subsidence analyses for conjugate sections across the Yucatan-Florida conjugate margin. Earlier publications presented crustal-scale interpretations of the margins with some structural restorations shown (e.g., Pascoe et al., 2016; Pindell et al., 2014; Rowan, 2018). While informative, these earlier published restorations have schematic, or simple area-balance calculations (e.g., Izquierdo-Llavall et al., 2022) and have not included detailed restoration of the observed structures in the post-rift sediment cover or detailed subsidence modeling. In the following sections we compare the structure of the conjugate margins, we discuss implications for the Jurassic tectonomorphic setting that facilitated salt deposition, we discuss dynamic topography in southeast North America, and finally present an interpretation of the tectonic setting during formation of the GoM basin.

### 6.1. Summary of Sections—Similarities in Conjugates

The pattern of Mesozoic deposition in deep water suggests that during the Jurassic, the region overlying the salt basin was subsiding, generating space for significant sedimentation. By the Cretaceous, the locus of deposition

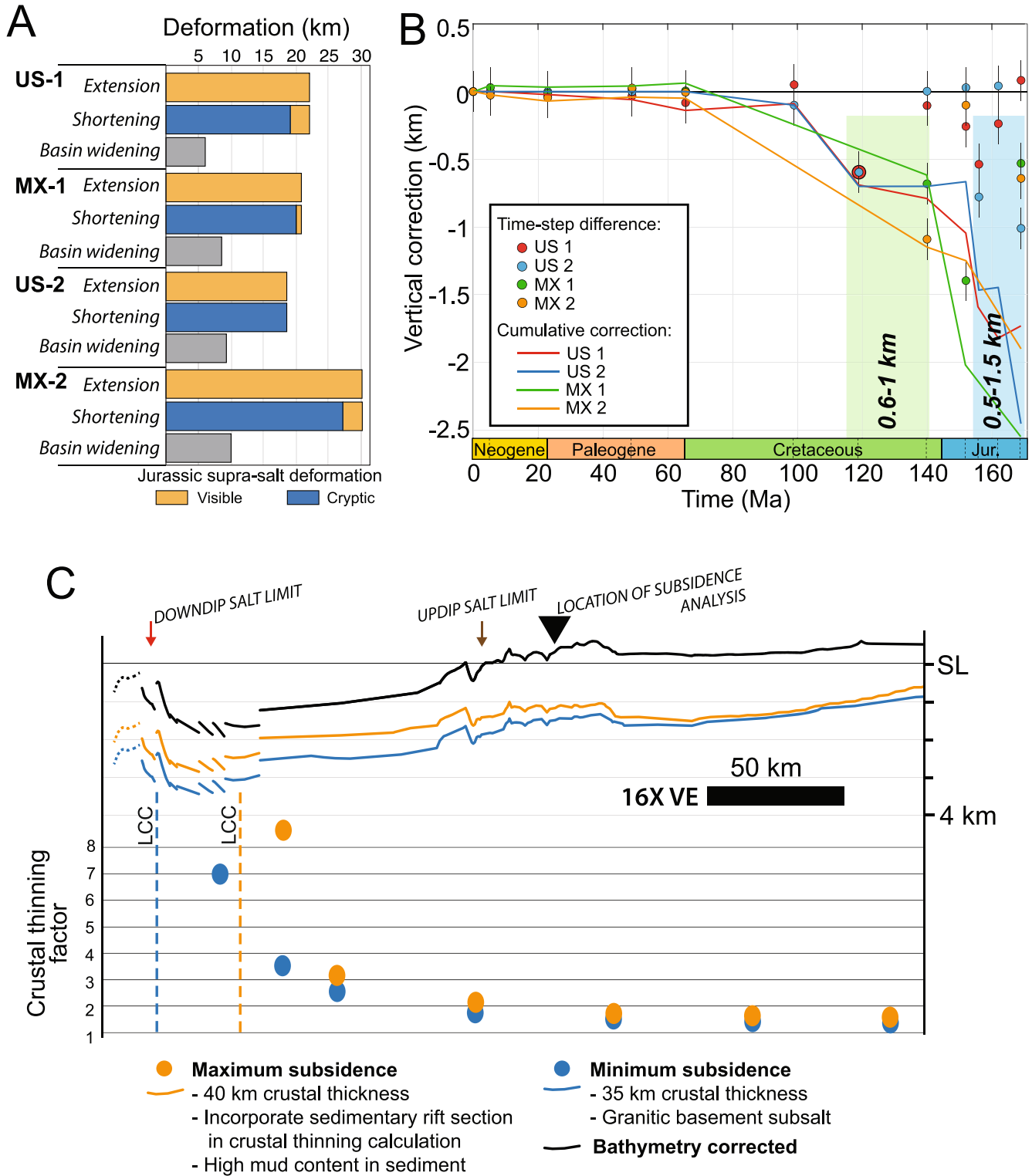


**Figure 8.** (a) Visible (yellow) and cryptic (blue) supra-salt extension/shortening and basin widening for each restoration. (b) Vertical corrections applied at each stage of the restoration (dots) and cumulatively (lines). (c) Maximum and minimum subsidence due to varying crustal and sedimentary parameters for line US-1. Upper panel: lines represent base of salt after restoration. Maximum subsidence (orange line) uses a 40 km original crustal thickness, includes a subsalt sedimentary rifted section, and increases the mud content by a factor of 2.5. Minimum thermal subsidence (blue line) uses a 35 km thick original crustal thickness and a granitic basement. Black line is bathymetry corrected where the updip pinchout of salt is at sea level. Dashed lines are in exhumed mantle/lower crust. Updip and downdip limits of salt are indicated, as well as location of subsidence analysis. Lower panel: dots show crustal thinning factors along-section, colors match the lines. LCC = Limit of Continental Crust. See Figure S4 in Supporting Information S1 for more details on crustal thickness measurements, thinning factors, and thermal subsidence for each line.



shifted toward the deeper water and/or carbonate platform (Figures 5 and 6). Jurassic deposition in the south-eastern proto-GoM was thickest toward the basin center, evident by ~4 km of Jurassic stratigraphy on conjugate lines US-2 and MX-2 compared to <3 km on conjugate lines US-1 and MX-1. This pattern of deposition may be indicative of greater subsidence in the central GoM due to (a) salt tectonics (greater original salt thickness), (b) nature of the pre-salt section, for example, differential compaction driven by a crystalline versus sedimentary subsalt lithology, and/or (c) differences in tectonic or thermal accommodation. In the absence of clear data suggesting such a tectonic mechanism, we cannot rule out large-scale tectonic accommodation, perhaps achieved by asymmetric extension as crustal breakup continued. However, we note that the thickest original salt and Jurassic section can be observed on both sides of the conjugate margin (US-2 and MX-2), suggesting that breakup asymmetry is not responsible for the Jurassic thickness variation.

We posit that a combination of salt tectonics and rifting dynamics are responsible for the Jurassic stratigraphy thickness variations. The presence of thick minibasins, extensional salt rollers, and the loci of Jurassic deposition on all studied lines support significant salt-induced subsidence. There is also a positive correlation between our interpreted cross-sectional area of the original salt basin and thickness of the post-salt Jurassic section, suggesting that breakup dynamics drove basin accommodation patterns throughout the Jurassic.

## 6.2. Summary of Sections—Salt Basin

Our systematic, sequential restorations provide the basis for a model of the original GoM conjugate margin salt basin and can be used to make inferences about the paleogeographic and tectonomorphic setting. Our results indicate a basin that widened from ~175 km in the southeast (sum of lines US-1 and MX-1, Figure 5d) to ~400 km in the east-central GoM (sum of lines US-2 and MX-2, Figure 6d). Based on guidelines laid out in Section 3.4, we interpret a deep salt basin (~2–2.5 km from the base of salt to global sea level) containing salt up to ~2 km thick in a depression ~1 km deep. Moving toward the central GoM, the basin deepened and salt thickened. These results are consistent with paleogeographic reconstructions, 3D seismic mapping, and deep-basin halite precipitation models (Peel, 2023; Sirota et al., 2020).

We observe discontinuous salt within continental crustal grabens, and subsequent stratigraphy overlapping oceanic crust/exhumed mantle (e.g., Figure 2b), indicative of syn-thinning and/or syn-mantle-exhumation salt deposition (Rowan, 2014). Our interpretation of the interaction between salt and Mesozoic sedimentation with outer trough structural relief indicates synchronous salt deposition with crustal deformation. We propose that during salt deposition and the latest stage of rifting, but prior to complete rupture, deformation was focused on crustal faults in highly thinned continental crust, likely including lower crustal exhumation. This tectonic setting produced structural relief in the most distal parts of the basin (Figure 4). We note that this structural interpretation is non-unique and does not necessarily apply to the entire GoM margin, where breakup was diachronous. There may be significant margin-parallel variations in magmatism and structural style that influence the exact structural evolution (Curry et al., 2018; Jian et al., 2021).

## 6.3. Deep-Basin Salt Deposition?

A key uncertainty in our reconstructions is the water depth in which Louann Salt was deposited—shallow (<100 m) or deep (>1 km). In the shallow scenario, the depositional surface was always close to sea level throughout salt deposition. Conversely, in the deep scenario, the base-salt surface could have been at a considerable depth (multi-km) below sea level in the center of the basin at the beginning of Louann deposition. This choice, which has a critical impact on the final stage of our reconstruction and the inferred rate of basement subsidence, was guided by consideration of modern and ancient analogs, the scientific literature, and local data constraints. This is an important question, and while it is not the focus of this paper, it is worthy of discussion.

Most modern evaporite-depositing systems, including sabkhas, playas and salinas, are shallow water (Warren, 2006). As a result, most geologists base interpretations of ancient evaporite deposits on such modern analogs (Schmalz, 1969). However, none of these modern, shallow water systems are capable of depositing halite giants comparable to those seen in the rock record, and their deposits are notably different from the Louann Salt. There is no modern analog for the salt giants seen in the geological record, for good reason: most salt giants formed at times with favorable plate configurations, such as supercontinent break-up, resulting in incipient rifts and narrow oceans within a supercontinent (e.g., Central and South Atlantic, Gulf of Mexico), or when plate

convergence isolates an oceanic basin (e.g., Messinian Mediterranean). Furthermore, they are often deposited during periods of high global temperature or aridity, or due to climate extremes enhanced by the existence of supercontinents, such as the IntraCambrian, Permian and Triassic (Warren, 2006). The study of modern evaporite systems is informative, but the present is not in this case the key to the past because evaporite-friendly plate geometries and global climate conditions do not exist today.

The modern Dead Sea, as the only modern deep water body precipitating halite, is a more useful analog to the ancient. Studies on the Dead Sea reveal a lot about processes of evaporite deposition and re-dissolution (Ouillon et al., 2019; Sirota et al., 2017, 2018, 2020), but the Dead Sea has several significant differences from ancient salt giants including scale, tectonic setting, the nature of water influx, and solute ion supply. The ancient record is more varied than the modern, and to make an environmental interpretation we must consider a wider range of possibilities than are expressed in modern analogs. Warren (2006) recognizes three main depth scenarios for the deposition of ancient salt giants; (a) deep water (>1 km), filled with hypersaline water, and a water surface near sea level; (b) deep basin, mostly dried out, with deposition below sea level in shallow brine at the basin bottom; (c) shallow basin, with shallow water near sea level.

The deep water scenario has two important variations. One scenario is a steady-state model in which deep water depth is maintained throughout the period of deposition by continual marine recharge, as set out in detail by Schmalz (1969). The steady state deep water model predicts deposition of a single-sequence evaporite deposit whose composition slowly changes as the deep basin becomes more concentrated. The relationship between concentration factor, water depth and depositional thickness can be readily calculated (Figure S5 in Supporting Information S1).

The alternative scenario is cyclic drawdown, where a basin may be refilled intermittently, then isolated and dessicated (Hsü, 1972; Tucker, 1991). This gives rise to a characteristic layered evaporite sequence (LES) as seen in the Aptian salt of the Campos Basin (Gambôa et al., 2008; Rodriguez et al., 2018). Each drawdown event lays down a succession of evaporite layers in order of solubility (commonly carbonate/anhydrite/halite/polyhalite/bittern salts) as the brine becomes concentrated (Usiglio J., 1849). Layered evaporites, consisting of stacked Usiglio Sequences, are diagnostic of evaporites deposited by cyclic flooding and drawdown (Davison et al., 2012) and they are readily identifiable in seismic and well data (e.g., Gamboa et al., 2008).

Deep water interpretations of ancient evaporite systems are long established in the literature; for example, the Zechstein Basin (Hsü, 1972; Ochseneus, 1877, 1978), the Salina salt, Michigan (Dellwig, 1955), and the Prairie Evaporite, Saskatchewan (Wardlaw & Schwerdtner, 1966). In some evaporite basins, deep water depth is unequivocally defined by high-relief bathymetric features that existed in the basin at the onset of evaporite deposition. For example, the height of the Capitan carbonate shelf margin of the Permian Basin, Texas, beneath the Castile evaporite, defines water depth of 0.5–1 km (Garber et al., 1989) and the Tenghiz carbonate platform draped by Kungurian salt defines >1 km water depth in the Pricaspian Basin, Kazakhstan (Harris et al., 2005).

Scenarios for deposition of giant evaporite deposits depend on three main options: (a) variations in water supply (continuous supply and steady-state salt precipitation, vs. intermittent supply and cyclic desiccation), (b) basin depth (deep vs. shallow), and (c) water depth (deep vs. shallow). With regards to water supply, well and seismic data indicate that the Louann Salt is not a layered evaporite sequence, consisting instead for the most part of a massive halite with minor anhydrite and rare potassium salts, with no visible depositional layering away from the basin margins (Fredrich et al., 2007). The absence of Usiglio Sequences in the Louann is compelling evidence against a cyclic drawdown scenario, instead supporting the steady-state deep water model.

Basin depth and water depth are more contentious. We refer the reader to Hudec and Peel (2019) for a summary of scenarios. Some authors have expressed a preference for a shallow-water model for Louann deposition (Pindell & Heyn, 2022; Pindell & Kennan, 2009; Pindell et al., 2014, 2021). These authors postulate slow deposition in a shallow water layer, with evaporite accumulation keeping pace with basement subsidence, but no direct geological evidence is presented for this preference. Other authors interpret a deep-water setting for Louann deposition (Peel, 2019, 2023; Rowan, 2018) away from the basin margins.

Seismic mapping and evaporite composition provide two lines of evidence for a deep-water model. Detailed 3D seismic mapping by the authors (Peel, 2023) demonstrates the existence of substantial paleotopography on the base-Louann Salt surface, indicating a deep water setting ( $\geq 2$  km water depth) at the onset of Louann deposition. Furthermore, by comparison with published charts of mineralogy versus evaporative concentration factor

(Schmalz, 1969; Usiglio, 1849; Warren, 2016, 2021) the observed mineralogy of the Louann (anhydrite, halite, minor K-salts; Fredrich et al., 2007) is compatible with a relatively low evaporative concentration factor ( $<70$ ), necessitating water depths  $\geq 1,500$  m to deposit salt 1–2 km thick (see Supporting Information S1).

In summary, deep-water deposition of the Louann Salt is not universally accepted, but there is a mounting body of evidence that it was the case. This has major implications for our analysis because it allows for basement subsidence to begin sooner and to progress more slowly than is required by the shallow-water model of Pindell et al. (2014) and Pindell and Heyn (2022), and it reduces the need for extremely rapid post-salt subsidence.

#### 6.4. Basin Widening/Cryptic Deformation

A key tenet of structural restorations with linked extensional-shortening domains is the amount of extension and contraction should be equal. We measure between 18 and 30 km of supra-salt extension on the sections with  $\sim 3$  km of equivalent downdip shortening, indicating 18–27 km of mismatch. We propose two explanations for this discrepancy: (a) shortening of precursor salt diapirs and (b) widening of the salt basin via post-salt salt flow or basement extension (e.g., Pichel et al., 2022).

Salt diapirs create a unique situation that makes it harder to document equivalence between updip extension and downdip contraction. They can “hide” deformation by squeezing and contracting. There is evidence for diapirism in all our presented sections and we depict widening and shortening diapirs as part of the restorations (Figures 5 and 6). We posit that this salt movement is responsible for some of the cryptic shortening we observe but precise measurements through time are purely speculative.

Widening of the salt basin changes the computation of extension and shortening by moving the backstop; salt-basin widening would create extension in the salt cover without the need for compensated shortening. Our restorations indicate between 6 and 10 km of salt-basin widening, representing 30%–50% of the cryptic shortening. These values are maximum estimates; they represent the distance between the reconstructed downdip limit of continental crust and the modern downdip extent of salt. Pichel et al. (2022) used thermo-mechanical geodynamic modeling to investigate post-rift salt flow and conclude that most up-dip extension is balanced by diapir shortening and is largely unrelated to downdip salt nappe advance. Nevertheless this widening may be propelled by continuing basement extension and/or gravitationally driven allochthonous salt flow in the downdip region due to differential thermal subsidence (e.g., on MX-1 and MX-2; Brun & Fort, 2011). The structural relief observed in the outer trough on all sections is indicative of ongoing tectonism during and immediately following salt deposition. All post-salt basement extension appears to be focused basinward, in the outer trough. We observe little evidence for post-salt basement extension in the more proximal stretches of the cross-sections (i.e., immediately below the salt, e.g., Rowan, 2018). Overall, the amount of post-salt basin widening we interpret is relatively small. However, it is sufficient to (a) create local accommodation space for salt to flow, and (b) marginally increase the gravitational potential energy. These are favorable conditions for gravitational salt flow, facilitating supra-salt extension. In summary, we suggest that the observed imbalance between updip salt-detached extension and downdip salt-detached shortening can be explained by a combination of diapir shortening and salt basin widening via ongoing tectonism in the outer trough.

#### 6.5. Anomalous Subsidence

As described in Section 3.2, our restorations account for structural deformation, compaction, flexural isostasy, and post-extensional thermal subsidence. In 2D Move<sup>TM</sup>, stretching is laterally variable but vertically invariant, represented by a lithosphere extension factor  $\beta$ , (sensu McKenzie, 1978). Paleobathymetry predicted using this approach is a good match to the geological data for the Late Cretaceous to Recent, but there is a significant discrepancy for the older reconstructions. The predicted, model-derived, bathymetry is too deep by 500–1,500 m in the Late Jurassic and 600–1,000 m in Early Cretaceous (Figure 8). This apparent anomaly is seen on both margins, but it appears to be larger on the Mexican margin.

Excess subsidence, seen in many basins around the world (e.g., Morley & Westaway, 2006; Vibe et al., 2018; Zhao et al., 2013), is commonly explained by depth-dependent thinning (DDT) and dynamic topography. DDT involves decoupled lithospheric layers (upper crust, lower crust, lithospheric mantle) thinning asynchronously and/or by different amounts (Huismans & Beaumont, 2008; Lavier & Manatschal, 2006; Royden & Keen, 1980).

DDT can have significant effects on basin subsidence; for example, if mantle thinning outpaces crustal thinning, post-rift subsidence will be greater than syn-rift (Svartman Dias et al., 2016). Furthermore, extension could be equivalent in all lithospheric layers, but be distributed over different widths, which would produce spatially variable subsidence trends (White & McKenzie, 1988). Filina and Beutel (2021) interpret significant differences in upper and lower crustal stretching in the GoM. The scale of anomalous Mesozoic subsidence found in this study is of the same magnitude as post-rift DDT-driven subsidence interpreted elsewhere (Morley & Westaway, 2006; Zhao et al., 2013).

Dynamic topography related to mantle flow is another potential source of anomalous uplift and subsidence. Upward flow of the mantle both supports and heats the overlying lithosphere, producing anomalous elevation up to 2 km (Davies et al., 2023; Gurnis, 1993; Hoggard et al., 2016). When the upwelling wanes, or shifts laterally relative to the lithosphere, the previously elevated region experiences subsidence unrelated to lithospheric stretching. Dynamic topography results from mantle flow at a range of spatio-temporal scales and intensities including superswells (East et al., 2020), hotspots originating at the core/mantle boundary, and circulation in the upper mantle only (Richards et al., 2020). Not all dynamic uplifts are hotspots, but all hotspots produce dynamic uplift.

It has been proposed that the transient presence of a mantle hotspot drove dynamic topography in the study area. Burke and Torsvik (2004) note that a known hotspot, currently located in the central Atlantic, which is variously known as the CAMP hotspot (Reeves, 2010) or the Sierra Leone Hotspot (Basile et al., 2020), would have been located at the center of the Central Atlantic Magmatic Province (CAMP) at the peak of CAMP magmatic activity around 201 Ma (Davies et al., 2017; Marzoli et al., 2018). Basile et al. (2020) note that periods of heightened activity on this hotspot are consistent with observed magmatism in the Demarara Plateau (170–180 Ma) and the Guinea Plateau (ca. 165 Ma). Reconstructions presented by Reeves (2010) indicate transient passage of this hotspot under Florida and the eastern GoM at 180–190 Ma. Pindell and Heyn (2022) proposed that anomalous uplift followed by subsidence of the eastern GoM margin may have been dynamic topography, caused by the arrival and subsequent departure of this hotspot under the region. The post-Louann onset of subsidence (i.e., after 170 Ma) in the eastern GoM as proposed by Pindell and Heyn (2022) is problematic; Reeves (2010) shows the hotspot having left the region 10 Myr previously, by 180 Ma while Basile et al. (2020) show it already at the Demarara Plateau by 170–180 Ma.

Our results provide strong, quantitative evidence of 1–2 km of anomalous uplift followed by subsidence, consistent in timing, location and magnitude with both DDT and transient dynamic uplift; we suggest that both mechanisms contributed, but we are not currently able to separate their effect. Our interpretation of the Louann Salt as a deep water basin allows for the subsidence to begin significantly earlier, prior to salt deposition (pre-170 Ma) rather than beginning after salt deposition, as suggested by Pindell and Heyn (2022). This timing is a better fit to the presence of the CAMP/Sierra Leone hotspot under Florida ca. 180–190 Ma (Basile et al., 2020; Reeves, 2010).

## 6.6. Early GoM Evolution

We offer an interpretation of the early stages of breakup in the GoM. Our interpretation is based on seismic interpretation presented in this contribution, and paleogeography research (Peel, 2023). We refer readers to the thorough review by Filina and Beutel (2021) for a detailed description of GoM tectonics. Prior to salt deposition the study area was a broad, deep, extensional basin. There are no well penetrations of the pre-salt section in the deep water. Previous interpretations of the pre-salt conditions (e.g., Salvador, 1991), which consider the presalt section to consist mostly of red beds and volcanics laid down in arid conditions, are largely based on outcrops and wells around the basin fringes. However, seismic mapping shows that the presalt section in the deeper basin is different in thickness, age, and seismic facies from the margins (e.g., Figure 4). Thus, the environment of deposition of this section is likely different. Increasing observations of semi-transparent seismic facies and depositional structures, including clinoforms and growth strata, suggest that immediate pre-salt deposition (the UPM) was dominated by deepwater siliciclastic material in the basin center (Filina & Hartford, 2021; Izquierdo-Llavall et al., 2022; Williams-Rojas et al., 2012). Pre-salt sedimentary basins are also supported by magnetic and gravity observations (Filina & Beutel, 2021).

In the north, the UPM is broken by basin-dipping normal faults that are absent in the south, indicating that at the time of salt deposition the basin was late-syn-rift in the north but late- or post-rift in the south. This asymmetry

in the sub-salt GoM is also evident in the widths of oceanic crust and interpreted magmatic input (Filina & Beutel, 2021). We interpret that salt was deposited in a syn-thinning or early syn-exhumation basin (in terminology of Rowan (2014)), prior to oceanic crust emplacement. We note that due to the extremely rapid timespan for salt deposition (<100 ka; Peel, 2023) and diachronous nature of crustal split in the GoM, this timing may not apply to entire margin. For example, it is feasible that elsewhere in the GoM crustal thinning/oceanic crust emplacement was more/less developed at the time of salt deposition.

Lack of a seismic Moho between clear oceanic crust and continental crust suggests the presence of exhumed lower crust or mantle at this transition. Filina and Beutel (2021) report integration of potential fields and seismic data to support a lower crustal nature for this region rather than mantle. Here, the base of the UPM, LPM, and continental crust is a fault that exhumes lower crust. Lower crustal exhumation produced relief and extension in the outer trough that influenced salt flow and facilitated basin widening. The first post-salt stratigraphy (Norphlet equivalent/Sakarn) onlaps exhumed lower crustal rock; these growth strata confirm concomitant sedimentation and exhumation (Figures 2b and 6). The first Jurassic interval clearly deposited on oceanic crust is the Haynesville-Buckner (HVB) equivalent, which dates full crustal split to the Late Jurassic (Kimmeridgian, ca. 150 Ma) (Snedden et al., 2014).

### 6.7. Limitations

This work is based on state of the art seismic images and well data that are used to conduct structural restorations, while incorporating well-established models for various subsidence mechanisms (decompaction, flexural, and rift-related thermal subsidence). We have strived to accurately represent limitations of the data, models, and interpretations while also presenting a range of possible scenarios. Below we describe some of the major limitations of our workflow.

Due to the two-phase, rotational component of extension in the Gulf of Mexico and temporal changes in sediment transport, it is impossible to situate cross-sections perfectly perpendicular to the transport direction from rifting to present, which is ideal for structural restorations. We are further limited by location of existing, high-quality, depth-migrated seismic data. Many of these limitations are minimized by the enormous body of work documenting the geology of the GoM, for example, deep seismic data that image the Moho and thousands of wells that document lithology. The seismic and well data that form the basis for this work are high quality and expensive to collect, providing a rare, high-resolution basis for our analysis.

This work utilizes Move™ software (Move Suite, 2016) which incorporates particular calculations for back-stripping, flexural isostasy, and thermal subsidence algorithms. These models, like all numerical models, have limitations. In particular, the parameters used will obviously influence the results. We have attempted to capture a full range of possible subsidence scenarios by undertaking the sensitivity analysis (Section 5.4, Figure 8c; Figure S4 in Supporting Information S1) where we explore (a) variable crustal parameters that will effect thermal subsidence and (b) lithologic variability that may effect decompaction. A particular limitation of our approach is the inability to consider depth-dependent stretching, which is a potential mechanism for post-rift subsidence.

We have presented evidence and arguments related to paleo-elevations in the early stages of GoM rifting, and acknowledge uncertainty in the precision and accuracy of our interpretations. The precise density and thermal structure of the distal margin during crustal breakup and salt deposition is exceedingly difficult to constrain and has implications for the rift-to-drift interpretation. Our strongest paleo-bathymetric constraints are for the Mesozoic platform carbonates, which is also the time period where the greatest subsidence anomalies are observed. While the paleoelevation of the distal margin is more interpretive, the overall observations of anomalous vertical movements identified in the proximal margin where constraints are strong are robust.

## 7. Conclusion

We present an interpretation of the US-Mexico conjugate margin salt basin. Our interpretation is based on sequential, balanced structural restorations and subsidence analyses that rely on high-quality and high-resolution seismic and well data. Based on evaporite composition and seismic mapping we favor a deep-water halite deposition model for the Louann Salt, reducing the need for rapid post-salt subsidence. We describe a salt basin that widens and thickens toward the central GoM, with original salt thicknesses in our study area of ~1–2 km. Our restorations

document significant cryptic deformation whereby extension and shortening are not balanced due to salt tectonics and basin widening. Subsidence analyses from the proximal margin reveal consistent anomalous vertical movements totaling 1–2 km in the mid-late Mesozoic; this subsidence could be the result of depth-dependent stretching and/or dynamic topography. Finally, we present a model for the early GoM based on our analysis that suggests pre-salt clastic sedimentation followed by salt deposition in a deep-water basin. We suggest that lower crustal exhumation facilitated crustal breakup and salt deposition occurred in a syn-thinning or early syn-exhumation basin.

## Data Availability Statement

The data used in this publication include seismic images from TGS Geophysical. These images are available for purchase from TGS Geophysical (<https://www.tgs.com/>). For the restorations we use the software Move by Petroleum Experts, which is available for purchase (<https://www.petex.com/products/ipm-suite/move-suite/>).

## Acknowledgments

The authors acknowledge the AGL and GBDS Industrial Associates Programs at The University of Texas Jackson School of Geoscience for making this research possible. Seismic images courtesy of TGS. Move software provided by Petroleum Experts. Thanks to Annie Walker for assistance with the GBDS database. We also thank Oliver Duffy for useful discussions while conducting the restorations, and Sarah Gelman for thoughtful discussions on thermal subsidence. We thank Chris Connors, Jim Pindell, and two anonymous reviewers for their comments on an earlier version of this paper, which improved the manuscript.

## References

- Allen, P. A., & Allen, J. R. (2004). *Basin analysis: Principles and applications* (p. 560). Blackwell Publishing Ltd.
- Augustin, N., Devey, C. W., van der Zwan, F. M., Feldens, P., Tominaga, M., Bantan, R. A., & Kwasnitschka, T. (2014). The rifting to spreading transition in the Red Sea. *Earth and Planetary Science Letters*, 395, 217–230. <https://doi.org/10.1016/j.epsl.2014.03.047>
- Babel, M., & Schreiber, B. C. (2014). Geochemistry of evaporites and evolution of seawater. In *Treatise on geochemistry* (Vol. 9, pp. 483–560). Elsevier. <https://doi.org/10.1016/B978-0-08-095975-7.00718-X>
- Basile, C., Girault, I., Paquette, J.-L., Agranier, A., Loncke, L., Heuret, A., & Poetisi, E. (2020). The Jurassic magmatism of the Demerara Plateau (offshore French Guiana) as a remnant of the Sierra Leone hotspot during the Atlantic rifting. *Scientific Reports*, 10(1), 7486. <https://doi.org/10.1038/s41598-020-64333-5>
- Brun, J.-P., & Fort, X. (2011). Salt tectonics at passive margins: Geology versus models. *Marine and Petroleum Geology*, 28(6), 1123–1145. <https://doi.org/10.1016/j.marpetgeo.2011.03.004>
- Buffler, R. T. (1980). Geologic history of deep Gulf of Mexico Basin. *AAPG Bulletin*, 64, 1277–1278. <https://doi.org/10.1306/2F919486-16CE-11D7-8645000102C1865D>
- Burke, K., & Torsvik, T. H. (2004). Derivation of Large Igneous Provinces of the past 200 million years from long-term heterogeneities in the deep mantle. *Earth and Planetary Science Letters*, 227(3–4), 531–538. <https://doi.org/10.1016/j.epsl.2004.09.015>
- Costa, E., & Vendeville, B. C. (2002). Experimental insights on the geometry and kinematics of fold-and-thrust belts above weak, viscous evaporitic décollement. *Journal of Structural Geology*, 24(11), 1729–1739. [https://doi.org/10.1016/S0191-8141\(01\)00169-9](https://doi.org/10.1016/S0191-8141(01)00169-9)
- Curry, M. A. E., Peel, F. J., Hudec, M. R., & Norton, I. O. (2018). Extensional models for the development of passive-margin salt basins, with application to the Gulf of Mexico. *Basin Research*, 30(6), 1180–1199. <https://doi.org/10.1111/bre.12299>
- Davies, D. R., Ghelichkhan, S., Hoggard, M. J., Valentine, A. P., & Richards, F. D. (2023). Observations and models of dynamic topography: Current status and future directions. In J. C. Duarte (Ed.), *Dynamics of plate tectonics and mantle convection* (pp. 223–269). Elsevier. <https://doi.org/10.1016/B978-0-323-85733-8.00017-2>
- Davies, J. H. F. L., Marzoli, A., Bertrand, H., Youbi, N., Ernesto, M., & Schaltegger, U. (2017). End-Triassic mass extinction started by intrusive CAMP activity. *Nature Communications*, 8(1), 15596. <https://doi.org/10.1038/ncomms15596>
- Davison, I., Anderson, L., & Nuttall, P. (2012). Salt deposition, loading and gravity drainage in the Campos and Santos salt basins. In G. I. Alsop, S. G. Archer, A. J. Hartley, N. T. Grant, & R. Hodgkinson (Eds.), *Salt Tectonics, Sediments and Prospectivity*. (Vol. 363(1), pp. 159–174). Geological Society of London. <https://doi.org/10.1144/SP363.8>
- Dellwig, L. F. (1955). Origin of the Salina salt of Michigan. *Journal of Sedimentary Research*, 25, 83–110. <https://doi.org/10.1306/D4269819-2B26-11D7-8648000102C1865D>
- Dooley, T. P., Jackson, M. P. A., & Hudec, M. R. (2015). Breakout of squeezed stocks: Dispersal of roof fragments, source of extrusive salt and interaction with regional thrust faults. *Basin Research*, 27(1), 3–25. <https://doi.org/10.1111/bre.12056>
- Dooley, T. P., Jackson, M. P. A., Hudec, M. R., & Dooley, T. P. (2013). Coeval extension and shortening above and below salt canopies on an uplifted, continental margin: Application to the northern Gulf of Mexico. *AAPG Bulletin*, 97(10), 1737–1764. <https://doi.org/10.1306/03271312072>
- Dynamic Data Services. (2012). *Dynamic data services*. SuperCache. Retrieved from <https://www.dynpg.com/supercache-2d>
- East, M., Müller, R. D., Williams, S., Zahirovic, S., & Heine, C. (2020). Subduction history reveals Cretaceous slab superflux as a possible cause for the mid-Cretaceous plume pulse and superswell events. *Gondwana Research*, 79, 125–139. <https://doi.org/10.1016/j.gr.2019.09.001>
- Eddy, D. R., Van Avendonk, H. J. A., Christeson, G. L., Norton, I. O., Karner, G. D., Johnson, C. A., & Snedden, J. W. (2014). Deep crustal structure of the northeastern Gulf of Mexico: Implications for rift evolution and seafloor spreading. *Journal of Geophysical Research: Solid Earth*, 119(9), 6802–6822. <https://doi.org/10.1002/2014JB011311>
- Ewing, T. E., & Galloway, W. E. (2019). Evolution of the northern Gulf of Mexico sedimentary basin. In *The sedimentary basins of the United States and Canada* (pp. 627–694). Elsevier. <https://doi.org/10.1016/B978-0-444-63895-3.00016-4>
- Feldens, P., & Mitchell, N. C. (2015). Salt flows in the central Red Sea. In N. M. A. Rasul, & I. C. F. Stewart (Eds.), *The Red Sea* (pp. 205–218). Springer Earth System Sciences. [https://doi.org/10.1007/978-3-662-45201-1\\_12](https://doi.org/10.1007/978-3-662-45201-1_12)
- Filina, I., Austin, J., Doré, T., Johnson, E., Minguez, D., Norton, I., et al. (2022). Opening of the Gulf of Mexico: What we know, what questions remain, and how we might answer them. *Tectonophysics*, 822, 229150. <https://doi.org/10.1016/j.tecto.2021.229150>
- Filina, I., & Beutel, E. (2021). Geological and geophysical constraints guide new tectonic reconstruction of the Gulf of Mexico. In I. Cemen, & E. Catlos (Eds.), *Tectonic processes: A global view, volume 1. Extensional tectonics: Continental breakup to formation of oceanic basins* (Vol. 1). John Wiley & Sons Inc. <https://doi.org/10.1002/essoar.10511463.1>
- Filina, I., & Hartford, L. (2021). Subsurface structures along western Yucatan from integrated geophysical analysis. *Marine and Petroleum Geology*, 127, 104964. <https://doi.org/10.1016/j.marpetgeo.2021.104964>
- Frazier, D. E. (1974). *Depositional episodes: Their relationship to the Quaternary stratigraphic framework in the northwestern portion of the Gulf Basin* (Vol. 71–1). The University of Texas at Austin, Bureau of Economic Geology Geological Circular.

- Fredrich, J. T., Fossum, A. F., & Hickman, R. J. (2007). Mineralogy of deepwater Gulf of Mexico salt formations and implications for constitutive behavior. *Journal of Petroleum Science and Engineering*, 57(3–4), 354–374. <https://doi.org/10.1016/j.PETROL.2006.11.006>
- Galloway, W. E. (2008). Depositional evolution of the Gulf of Mexico sedimentary basin. In A. D. Miall, & K. J. Hsu (Eds.), *Sedimentary basins of the world: Sedimentary basins of the United States and Canada* (Vol. 5, pp. 505–549). Elsevier. [https://doi.org/10.1016/S1874-5997\(08\)00015-4](https://doi.org/10.1016/S1874-5997(08)00015-4)
- Galloway, W. E., Ganey-Curry, P. E., Li, X., Buffler, R. T., & Galloway, W. (2000). Cenozoic depositional history of the Gulf of Mexico basin. *AAPG Bulletin*, 84(11), 1743–1774. <https://doi.org/10.1306/8626c37f-173b-11d7-8645000102c1865d>
- Gambôa, L., Machado, M. A. P., Silveira, D. P., Freitas, J. T. R., & Silva, S. R. P. (2008). Evaporitos estratificados no Atlântico Sul: interpretação sísmica e controle tectono-estratigráfico na Bacia de Santos. In *Sa: Geologia e Tectônica, Exemplos nas Básicas Brasileiras* (pp. 340–359).
- Garber, R. A., Grover, G. A., & Harris, P. M. (1989). Geology of the Capitan shelf margin—Subsurface data from the northern Delaware Basin. In P. M. Harris, & G. A. Grover (Eds.), *Subsurface and outcrop examination of the capitan shelf margin, northern Delaware basin* (pp. 3–271). SEPM (Society for Sedimentary Geology). <https://doi.org/10.2110/COR.89.13.0003>
- Goteti, R., Beaumont, C., & Ings, S. J. (2013). Factors controlling early stage salt tectonics at rifted continental margins and their thermal consequences. *Journal of Geophysical Research: Solid Earth*, 118(6), 3190–3220. <https://doi.org/10.1002/jgrb.50201>
- Gurnis, M. (1993). Phanerozoic marine inundation of continents driven by dynamic topography above subducting slabs. *Nature*, 364(6438), 589–593. <https://doi.org/10.1038/364589a0>
- Handford, C. R., & Loucks, R. G. (1993). Carbonate depositional sequences and systems tracts—Responses of carbonate platforms to relative sea-level changes. In *Carbonate sequence stratigraphy: Recent developments and applications* (Vol. 57, pp. 3–41). AAPG Special Volumes Retrieved from <http://archives.datapages.com/data/specpubs/seismic2/data/a168/a168/0001/0000/0003.htm>
- Haq, B. U., Hardenbol, J., & Vail, P. R. (1987). Chronology of fluctuating sea levels since the Triassic. *Science*, 235(4793), 1156–1167. <https://doi.org/10.1126/science.235.4793.1156>
- Harris, P. M., Garber, R. A., & Clark, M. E. (2005). Geologic framework for the Tengiz and Korolev isolated carbonate platforms, Kazakhstan—Carboniferous isolated carbonate platforms: AAPG search and discovery. Article #20061.
- Heydari, E., Wade, W. J., & Anderson, L. C. (1997). Depositional environments, organic carbon accumulation, and solar-forcing cyclicity in Smackover Formation lime mudstones, northern Gulf Coast. *AAPG Bulletin*, 81(5), 760–774. <https://doi.org/10.1306/522b4839-1727-11d7-8645000102c1865d>
- Hoggard, M. J., White, N., & Al-Attar, D. (2016). Global dynamic topography observations reveal limited influence of large-scale mantle flow. *Nature Geoscience*, 9(6), 456–463. <https://doi.org/10.1038/ngeo2709>
- Hsü, K. J. (1972). Origin of saline giants: A critical review after the discovery of the Mediterranean evaporite. *Earth-Science Reviews*, 8(4), 371–396. [https://doi.org/10.1016/0012-8252\(72\)90062-1](https://doi.org/10.1016/0012-8252(72)90062-1)
- Hudec, M. R., Jackson, M. P. A., & Peel, F. J. (2013). Influence of deep Louann structure on the evolution of the northern Gulf of Mexico. *AAPG Bulletin*, 97(10), 1711–1735. <https://doi.org/10.1306/04011312074>
- Hudec, M. R., Jackson, M. P. A., & Schultz-Ela, D. D. (2009). The paradox of minibasin subsidence into salt: Clues to the evolution of crustal basins. *GSA Bulletin*, 121(2008), 201–221. <https://doi.org/10.1130/B26275.1>
- Hudec, M. R., & Norton, I. O. (2019). Upper Jurassic structure and evolution of the Yucatán and Campeche subbasins. *Southern Gulf of Mexico: AAPG Bulletin*, 103(5), 1133–1151. <https://doi.org/10.1306/11151817405>
- Hudec, M. R., Norton, I. O., Jackson, M. P. A., & Peel, F. J. (2013). Jurassic evolution of the Gulf of Mexico salt basin. *AAPG Bulletin*, 97(10), 1683–1710. <https://doi.org/10.1306/04011312073>
- Hudec, M. R., & Peel, F. J. (2019). A critical review of models for deposition of the Louann Salt, and implications for Gulf of Mexico evolution. In *GCSSEPM: Salt tectonics, associated processes, and exploration potential: Revisited* (pp. 222–238).
- Huerta, A. D., & Harry, D. L. (2012). Wilson cycles, tectonic inheritance, and rifting of the North American Gulf of Mexico continental margin. *Geosphere*, 8(2), 374–385. <https://doi.org/10.1130/GES00725.1>
- Huisman, R. S., & Beaumont, C. (2008). Complex rifted continental margins explained by dynamical models of depth-dependent lithospheric extension. *Geology*, 36(2), 163. <https://doi.org/10.1130/G24231A.1>
- Humphris, C. C., Jr. (1978). Salt movement on continental slope, northern Gulf of Mexico. In A. H. Bouma, G. T. Moore, & J. M. Coleman (Eds.), *Framework, facies, and oil trapping characteristics of the upper continental margin, American association of petroleum geologists studies in geology* (Vol. 7, pp. 69–85).
- Imbert, P. (2005). The Mesozoic opening of the Gulf of Mexico: Part 1, evidence for oceanic accretion during and after salt deposition. In *25th annual Gulf Coast section-SEPM foundation Bob F. Perkins research conference* (Vol. 25, pp. 1119–1150). Retrieved from <http://gcsproceedings.sepmonline.org/content/gcssepmproc/gcs025/1/SEC22.body.pdf>
- Izquierdo-Llavall, E., Ringenbach, J. C., Sapin, F., Rives, T., & Callot, J. P. (2022). Crustal structure and lateral variations in the Gulf of Mexico conjugate margins: From rifting to break-up. *Marine and Petroleum Geology*, 136, 105484. <https://doi.org/10.1016/j.marpetgeo.2021.105484>
- Jian, H., Nedimović, M. R., Canales, J. P., & Lau, K. W. H. (2021). New insights into the rift to drift transition across the northeastern Nova Scotian margin from wide-angle seismic waveform inversion and reflection imaging. *Journal of Geophysical Research: Solid Earth*, 126(12), e2021JB022201. <https://doi.org/10.1029/2021JB022201>
- Kirkham, C., Bertoni, C., Cartwright, J., Lensky, N. G., Sirota, I., Rodriguez, K., & Hodgson, N. (2020). The demise of a ‘salt giant’ driven by uplift and thermal dissolution. *Earth and Planetary Science Letters*, 531, 115933. <https://doi.org/10.1016/j.epsl.2019.115933>
- Lavrier, L. L., & Manatschal, G. (2006). A mechanism to thin the continental lithosphere at magma-poor margins. *Nature*, 440(7082), 324–328. <https://doi.org/10.1038/nature04608>
- Lawver, L., Dalziel, I., & Norton, I. (2017). PLATES project. Retrieved from <https://www.ig.utexas.edu/Marine-and-Tectonics/Plates-Project/>
- Liu, L. (2015). The ups and downs of North America: Evaluating the role of mantle dynamic topography since the Mesozoic. *Reviews of Geophysics*, 53(3), 1022–1049. <https://doi.org/10.1002/2015RG000489>
- Marton, G., & Buffler, R. T. (1994). Jurassic reconstruction of the Gulf of Mexico Basin. *International Geology Review*, 36(6), 545–586. <https://doi.org/10.1080/00206819409465475>
- Marzoli, A., Callegaro, S., Dal Corso, J., Davies, J. H. F. L., Chiaradia, M., Youbi, N., et al. (2018). The central Atlantic magmatic province (CAMP): A review. In L. H. Tanner (Ed.), *The late Triassic world: Earth in a time of transition* (pp. 91–125). Springer International Publishing. [https://doi.org/10.1007/978-3-319-68009-5\\_4](https://doi.org/10.1007/978-3-319-68009-5_4)
- McKenzie, D. (1978). Some remarks on the development of sedimentary basins. *Earth and Planetary Science Letters*, 40(1), 25–32. [https://doi.org/10.1016/0012-821X\(78\)90071-7](https://doi.org/10.1016/0012-821X(78)90071-7)
- Mitchell, N. C., Ligi, M., Ferrante, V., Bonatti, E., & Rutter, E. (2010). Submarine salt flows in the central Red Sea. *GSA Bulletin*, 122(5–6), 701–713. <https://doi.org/10.1130/B26518.1>

- Morley, C. K., & Westaway, R. (2006). Subsidence in the super-deep Pattani and Malay basins of southeast Asia: A coupled model incorporating lower-crustal flow in response to post-rift sediment loading. *Basin Research*, 18(1), 51–84. <https://doi.org/10.1111/j.1365-2117.2006.00285.x>
- Move Suite. (2016). Petroleum Experts [Software]. Retrieved from <https://www.petex.com/products/ipm-suite/move-suite/>
- Norton, I. O., Carruthers, D. T., & Hudec, M. R. (2016). Rift to drift transition in the South Atlantic salt basins: A new flavor of oceanic crust. *Geology*, 44(1), 55–58. <https://doi.org/10.1130/G37265.1>
- Ochsenius, K. (1877). *Die Bildung der Steinsalzlager und ihrer mutter augensalze*. C.E.M. Pfeffer.
- Ochsenius, K. (1978). On the formation of rock salt beds and mother liquor salts. In *Philadelphia academy of sciences* (pp. 181–187).
- Ouillon, R., Lensky, N. G., Lyakhovskiy, V., Arnon, A., & Meiburg, E. (2019). Halite precipitation from double-diffusive salt fingers in the Dead Sea: Numerical simulations. *Water Resources Research*, 55(5), 4252–4265. <https://doi.org/10.1029/2019WR024818>
- Pascoe, R., Nuttall, P., Dunbar, D., & Bird, D. (2016). Constraints on the timing of continental rifting and oceanic spreading for the Mesozoic Gulf of Mexico Basin. In C. M. Lowery, J. W. Snedden, & N. C. Rosen (Eds.), *35th Gulf Coast section-SEPM foundation Perkins-Rosen research conference* (pp. 81–122).
- Peel, F. (2019). Paleo-oceanographic preconditioning promotes precipitation: How the global context is a key factor for understanding Bajocian Louann salt deposition. In C. Fiduk, & N. C. Rosen (Eds.), *GCSSEPM: Salt tectonics, associated processes, and exploration potential: Revisited* (pp. 12–13). Gulf Coast Section SEPM Foundation.
- Peel, F. (2023). *A lost world rediscovered: 3D seismic data reveal spectacular images of a Jurassic landscape on the Eve of Louann salt deposition in the Gulf of Mexico, with implications for salt deposition*. AAPG Distinguished Lecturer Program. Retrieved from <https://www.aapg.org/career/training/in-person/distinguished-lecture/presentation/articleid/64702/frank-peel-a-lost-world-rediscovered-3d-seismic-data-reveal-spectacular-images-of-a-jurassic-landscape-on-the-eve-of-louann-salt-depositi>
- Peel, F. J., Travis, C. J., & Hossack, J. R. (1995). Genetic structural provinces and salt tectonics of the Cenozoic offshore U.S. Gulf of Mexico: A preliminary analysis. In M. P. A. Jackson, D. G. Roberts, & S. Snelson (Eds.), *Salt tectonics: A global perspective: AAPG memoir 65* (pp. 153–175).
- Pichel, L. M., Huisman, R. S., Gawthorpe, R., Faleide, J. I., & Theunissen, T. (2022). Late-syn- to post-rift salt tectonics on wide rifted margins—Insights from geodynamic modeling. *Tectonics*, 41(8). <https://doi.org/10.1029/2021TC007158>
- Pilcher, R. S., Murphy, R. T., & McDonough Ciosek, J. (2014). Jurassic raft tectonics in the northeastern Gulf of Mexico. *Interpretation*, 2(4), SM39–SM55. <https://doi.org/10.1190/INT-2014-0058.1>
- Pindell, J., & Dewey, J. F. (1982). Permo-Triassic reconstruction of western Pangea and the evolution of the Gulf of Mexico/Caribbean region. *Tectonics*, 1(2), 179–211. <https://doi.org/10.1029/TC001i002p00179>
- Pindell, J., Graham, R., & Horn, B. (2014). Rapid outer marginal collapse at the rift to drift transition of passive margin evolution, with a Gulf of Mexico case study. *Basin Research*, 26(6), 701–725. <https://doi.org/10.1111/bre.12059>
- Pindell, J., & Heyn, T. (2022). Dynamo-thermal subsidence and sag-section deposition as magma-rich rifted margins move off plume centres along incipient lines of break-up. *Journal of the Geological Society*, 179(5). <https://doi.org/10.1144/jgs2021-095>
- Pindell, J., Villagómez, D., Molina-Garza, R., Graham, R., & Weber, B. (2021). A revised synthesis of the rift and drift history of the Gulf of Mexico and surrounding regions in the light of improved age dating of the Middle Jurassic salt. In I. Davison, J. N. F. Hull, & J. Pindell (Eds.), *The Basins, Orogens, and Evolution of the Southern Gulf of Mexico and Northern Caribbean*. (Vol. 504(1), pp. 29–76). Geological Society. <https://doi.org/10.1144/SP504-2020-43>
- Pindell, J. L., & Kennan, L. (2009). Tectonic evolution of the Gulf of Mexico, Caribbean and northern South America in the mantle reference frame: An update. In K. H. James, M. A. Lorente, & J. L. Pindell (Eds.), *The origin and evolution of the Caribbean plate* (Vol. 328, pp. 1–55). Geological Society. <https://doi.org/10.1144/SP328.1>
- Pulham, A. J., Peel, F. J., Rives, T., Delph, B., Salel, J.-F., Nicholson, T., et al. (2019). The age of the Louann salt; insights from historic isotopic analyses in salt stocks from the onshore interior salt basins of the northern Gulf of Mexico. In *GCSSEPM: Salt tectonics, associated processes, and exploration potential: Revisited* (pp. 64–66).
- Reeves, C. (2010). Model CR10AALH. Retrieved from <https://www.reeves.nl/gondwana/large-igneous-provinces/>
- Richards, F. D., Hoggard, M. J., White, N., & Ghelichkhan, S. (2020). Quantifying the relationship between short-wavelength dynamic topography and thermomechanical structure of the upper mantle using calibrated parameterization of anelasticity. *Journal of Geophysical Research: Solid Earth*, 125(9), e2019JB019062. <https://doi.org/10.1029/2019JB019062>
- Rives, T., Pierin, A.-R., Pulham, A. J., Salel, J.-F., Wu, J., Duarte, A., & Magnier, B. (2019). The Sakarn series: A proposed new Middle Jurassic stratigraphic interval from the offshore eastern Gulf of Mexico. In *GCSSEPM: Salt tectonics, associated processes, and exploration potential: Revisited* (pp. 371–393).
- Rodriguez, C. R., Jackson, C. A. L., Rotevatn, A., Bell, R. E., & Francis, M. (2018). Dual tectonic-climatic controls on salt giant deposition in the Santos Basin, offshore Brazil. *Geosphere*, 14(1), 215–242. <https://doi.org/10.1130/GES01434.1>
- Rowan, M. (2017). The South Atlantic and Gulf of Mexico salt basins: Crustal thinning, subsidence and accommodation for salt and presalt strata. In K. R. McClay (Ed.), *The geological society special publications: Passive margins: Tectonics, sedimentation and magmatism*.
- Rowan, M. G. (2014). Passive-margin salt basins: Hyperextension, evaporite deposition, and salt tectonics. *Basin Research*, 26(1), 154–182. <https://doi.org/10.1111/bre.12043>
- Rowan, M. G. (2018). The South Atlantic and Gulf of Mexico salt basins: Crustal thinning, subsidence and accommodation for salt and presalt strata. In K. R. McClay, & J. A. Hammerstein (Eds.), *The geological society special publications: Passive margins: Tectonics, sedimentation and magmatism* (Vol. 476, p. 31). The Geological Society of London. <https://doi.org/10.1144/SP476.6>
- Rowan, M. G., Jackson, M. P. A., & Trudgill, B. D. (1999). Salt-related fault families and fault welds in the northern Gulf of Mexico. *AAPG Bulletin*, 83, 1454–1484. <https://doi.org/10.1306/e4fd41e3-1732-11d7-8645000102c1865d>
- Rowan, M. G., Peel, F. J., & Vendeville, B. C. (2004). Gravity-driven fold belts on passive margins. In K. R. McClay (Ed.), *Thrust tectonics and hydrocarbon systems: AAPG memoir 82* (pp. 157–182).
- Rowan, M. G., & Ratliff, R. A. (2012). Cross-section restoration of salt-related deformation: Best practices and potential pitfalls. *Journal of Structural Geology*, 41, 24–37. <https://doi.org/10.1016/j.jsg.2011.12.012>
- Rowan, M. G., Trudgill, B. D., & Carl Fiduk, J. (2000). Deep-water, salt-cored foldbelts: Lessons from the Mississippi Fan and Perdido foldbelts, northern Gulf of Mexico. In W. Mohriak, & M. Talwani (Eds.), *Atlantic rifts and continental margins: American geophysical union geophysical monograph 115* (pp. 173–191). American Geophysical Union. <https://doi.org/10.1029/GM115p0173>
- Royden, L., & Keen, C. E. (1980). Rifting process and thermal evolution of the continental margin of eastern Canada determined from subsidence curves. *Earth and Planetary Science Letters*, 51(2), 343–361. [https://doi.org/10.1016/0012-821X\(80\)90216-2](https://doi.org/10.1016/0012-821X(80)90216-2)
- Salvador, A. (1987). Late Triassic-Jurassic paleogeography and origin of Gulf of Mexico Basin. *AAPG Bulletin*, 71, 419–451. <https://doi.org/10.1306/94886ec5-1704-11d7-8645000102c1865d>



- Salvador, A. (1991). Triassic-Jurassic. In A. Salvador (Ed.), *DNAG, geology of North America: The Gulf of Mexico Basin*. U.S.A., Geological Society of America. <https://doi.org/10.1130/DNAG-GNA-J.131>
- Sawyer, D. S., Buffler, R. T., & Pilger, R. H., Jr. (1991). The crust under the Gulf of Mexico Basin. In A. Salvador (Ed.), *The Gulf of Mexico basin, the geology of North America* (pp. 53–72). Geological Society of America. <https://doi.org/10.1130/DNAG-GNA-J.53>
- Schmalz, R. F. (1969). Deep-water evaporite deposition: A genetic model. *AAPG Bulletin*, 53. <https://doi.org/10.1306/5D25C7FD-16C1-11D7-8645000102C1865D>
- Slater, J. G., & Christie, P. A. F. (1980). Continental stretching: An explanation of the post-mid-Cretaceous subsidence of the central North Sea basin. *Journal of Geophysical Research*, 85(B7), 3711–3739. <https://doi.org/10.1029/JB085iB07p03711>
- Sirota, I., Enzel, Y., & Lensky, N. G. (2017). Temperature seasonality control on modern halite layers in the Dead Sea: In situ observations. *Geological Society of America Bulletin*, 129(9–10), 1181–1194. <https://doi.org/10.1130/B31661.1>
- Sirota, I., Enzel, Y., & Lensky, N. G. (2018). Halite focusing and amplification of salt layer thickness: From the Dead Sea to deep hypersaline basins. *Geology*, 46(10), 851–854. <https://doi.org/10.1130/G45339.1>
- Sirota, I., Ouillon, R., Mor, Z., Meiburg, E., Enzel, Y., Arnon, A., & Lensky, N. G. (2020). Hydroclimatic controls on salt fluxes and halite deposition in the Dead Sea and the shaping of “salt giants”. *Geophysical Research Letters*, 47(22), e2020GL090836. <https://doi.org/10.1029/2020GL090836>
- Smith, J. E., & Santamarina, J. C. (2022). Red sea evaporites: Formation, creep and dissolution. *Earth-Science Reviews*, 232, 104115. <https://doi.org/10.1016/j.earscirev.2022.104115>
- Snedden, J. W., Cunningham, R. C., & Virdell, J. W. (2020). The northern Gulf of Mexico offshore super basin: Reservoirs, source rocks, seals, traps, and successes. *AAPG Bulletin*, 104(12), 2603–2642. <https://doi.org/10.1306/09092020054>
- Snedden, J. W., & Galloway, W. E. (2019). *The Gulf of Mexico sedimentary basin: Depositional evolution and petroleum applications*. Cambridge University Press. <https://doi.org/10.1017/9781108292795>
- Snedden, J. W., Norton, I. O., Christeson, G. L., & Sanford, J. C. (2014). Interaction of deepwater deposition and a mid-ocean spreading center, eastern Gulf of Mexico basin, USA. *Gulf Coast Association of Geological Societies Transactions*, 64, 371–383.
- Svartman Dias, A. E., Hayman, N. W., & Lavier, L. L. (2016). Thinning factor distributions viewed through numerical models of continental extension. *Tectonics*, 35(12), 3050–3069. <https://doi.org/10.1002/2016TC004266>
- TGS. (2016). [Seismic images]. *TGS Geophysical*. Retrieved from <https://www.tgs.com/>
- Tucker, M. E. (1991). Sequence stratigraphy of carbonate-evaporite basins: Models and application to the Upper Permian (Zechstein) of northeast England and adjoining North Sea. *Journal of the Geological Society*, 148(6), 1019–1036. <https://doi.org/10.1144/GSJGS.148.6.1019>
- Turcotte, D., & Schubert, G. (2014). *Geodynamics* (p. 623). Cambridge University Press.
- Usiglio, J. (1849). Étude de la composition de l'eau de la Méditerranée et sur l'exploitation des sels qu'elle contient. *Annales de Chimie et de Physique*, 3, 172–191.
- Vibe, Y., Bunge, H.-P., & Clark, S. R. (2018). Anomalous subsidence history of the West Siberian Basin as an indicator for episodes of mantle induced dynamic topography. *Gondwana Research*, 53, 99–109. <https://doi.org/10.1016/j.gr.2017.03.011>
- Wardlaw, N. C., & Schwerdtner, W. M. (1966). Halite-anhydrite seasonal layers in the Middle Devonian Prairie evaporite formation, Saskatchewan, Canada. *GSA Bulletin*, 77(4), 331–342. [https://doi.org/10.1130/0016-7606\(1966\)77\[331:HSLITM\]2.0.CO;2](https://doi.org/10.1130/0016-7606(1966)77[331:HSLITM]2.0.CO;2)
- Warren, J. K. (2006). *Evaporites: Sediments, resources and hydrocarbons*. Springer Berlin.
- Warren, J. K. (2016). Salt dissolution and pointers to vanished evaporites: Karst, Breccia, Nodules and Cement. In *Evaporites* (pp. 613–761). Springer International Publishing. [https://doi.org/10.1007/978-3-319-13512-0\\_7](https://doi.org/10.1007/978-3-319-13512-0_7)
- Warren, J. K. (2021). Evaporite Deposits. In *Encyclopedia of Geology* (pp. 945–977). Elsevier. <https://doi.org/10.1016/B978-0-08-102908-4.00165-X>
- White, N., & McKenzie, D. (1988). Formation of the “steer’s head” geometry of sedimentary basins by differential stretching of the crust and mantle. *Geology*, 16(3), 250. [https://doi.org/10.1130/0091-7613\(1988\)016<0250:FOTSSH>2.3.CO;2](https://doi.org/10.1130/0091-7613(1988)016<0250:FOTSSH>2.3.CO;2)
- Williams-Rojas, C. T., Reyes-Tovar, E., Miranda-Peralta, L., Reyna-Martinez, G., Cardenas-Alvarado, A., Maldonado-Villalon, R., et al. (2012). Hydrocarbon potential of the Deepwater Portion of the “Salina del Istmo” Province, Southeastern Gulf of Mexico, Mexico. In *Gulf Coast association of geological societies transactions*.
- Zhao, Z., Sun, Z., Wang, Z., Sun, Z., Liu, J., Wang, Z., & Sun, L. (2013). The dynamic mechanism of post-rift accelerated subsidence in Qiongdongnan Basin, northern South China Sea. *Marine Geophysical Research*, 34(3–4), 295–308. <https://doi.org/10.1007/s11001-013-9188-2>

## References From the Supporting Information

- Theunissen, T., Huisman, R. S., Lu, G., & Riel, N. (2022). Relative continent—Mid-ocean ridge elevation: A reference case for isostasy in geodynamics. *Earth-Science Reviews*, 233, 104153. <https://doi.org/10.1016/j.earscirev.2022.104153>